Mon. Not. R. Astron. Soc. **369,** 655–672 (2006) doi:10.1111/j.1365-2966.2006.10302.x

TEMPO2, a new pulsar-timing package – I. An overview

G. B. Hobbs,★ R. T. Edwards and R. N. Manchester
Australia Telescope National Facility, CSIRO, PO Box 76, Epping, NSW 1710, Australia

Accepted 2006 March 8. Received 2006 March 7; in original form 2006 January 24

ABSTRACT

Contemporary pulsar-timing experiments have reached a sensitivity level where systematic errors introduced by existing analysis procedures are limiting the achievable science. We have developed TEMPO2, a new pulsar-timing package that contains propagation and other relevant effects implemented at the 1-ns level of precision (a factor of ∼100 more precise than previously obtainable). In contrast with earlier timing packages, TEMPO2 is compliant with the general relativistic framework of the IAU 1991 and 2000 resolutions and hence uses the International Celestial Reference System, Barycentric Coordinate Time and up-to-date precession, nutation and polar motion models. TEMPO2 provides a generic and extensible set of tools to aid in the analysis and visualization of pulsar-timing data. We provide an overview of the timing model, its accuracy and differences relative to earlier work. We also present a new scheme for predictive use of the timing model that removes existing processing artefacts by properly modelling the frequency dependence of pulse phase.

Key words: methods: data analysis – ephemerides – pulsars: general.

1 INTRODUCTION

Pulsar-timing observations have produced some of the most exciting results in pulsar astronomy and indeed in all of astronomy. For instance, such results have included the first detection of extrasolar planets (Wolszczan & Frail 1992), stringent tests of the general theory of relativity (e.g. Stairs 2003), revealed dispersion-measure variations due to the interstellar medium (ISM) (e.g. Backer et al. 1993), pulsar proper motions (e.g. Hobbs et al. 2004) and irregularities in the spin-down of pulsars (e.g. Lyne 1999). Pulsar timing is now being used to verify terrestrial time standards and the Solar system ephemeris and in searches for gravitational radiation (see e.g. Foster & Backer 1990; Jenet et al. 2005).

An overview of pulsar timing has been given by numerous authors (e.g. Manchester & Taylor 1977; Backer & Hellings 1986; Lyne & Smith 1998; Lorimer & Kramer 2005). In brief, the arrival times of pulses (TOAs) are measured at a radio observatory for a particular pulsar over many years. These TOAs need adjustment so that they represent arrival times in an inertial reference frame. This is accomplished by transforming each measured arrival time to an arrival time in the reference frame of the pulsar by first calculating arrival times at the Solar system barycentre (SSB) and then, if necessary, including additional terms required to model the pulsar's orbital motion. A model of the pulsar's spin-down behaviour, the 'timing model' or 'timing ephemeris', is fitted to these arrival times. If significant systematic deviations are seen when calculating the differences between the actual arrival times and the best-fitting model arrival times (known as timing residuals), then it is clear that the model is not fully describing the true pulsar parameters; a positive residual corresponds to the pulse arriving later than predicted. Such discrepancies can be due to many effects including unmodelled binary companions or binary parameters, irregularities in the spin-down of the pulsar, or poor estimation of the astrometric or rotational parameters. For instance, an incorrect estimate of the pulsar's position or its proper motion leads to a poor determination of the barycentric arrival times, which will produce a sinusoidal feature in the timing residuals. This timing technique therefore allows pulsar parameters to be measured extremely precisely; the precision improves with longer data sets and more accurate TOA measurements.

Both the conversion from the measured TOAs to barycentric arrival times and the model fitting required to obtain precise pulsar parameters are complex and can only be carried out within a computer program. Programs such as PSRTIME at the Jodrell Bank Observatory, TIMAPR at Bonn, ANTIOPE at Nancay and CPHAS at Hartebeesthoek observatories have already been developed. However, the most widely used and best-known package is TEMPO which has been maintained and distributed by Princeton University and the Australia Telescope National Facility. [1] This package is extremely powerful, but the algorithms implemented are poorly documented and only provide a timing precision of ∼100 ns. Recent high-precision timing experiments produce root-mean-square (rms) residuals of this order and, therefore, such results are systematically affected by inaccuracies in the TEMPO algorithms. A further limitation of TEMPO is that it can only be used to analyse one pulsar at a time. In order to study the recently discovered double-pulsar system (Lyne et al. 2004), to search for gravitational waves or to look for irregularities in

★Email: george.hobbs@csiro.au

[1] http://www.atnf.csiro.au/research/pulsar/tempo.

terrestrial time standards, it is advantageous to analyse multiple pulsars simultaneously. We have developed a new package, known as TEMPO2, which is based on the original TEMPO (hereafter called TEMPO1), but has a significant number of new and improved features.

The aim of this paper is not to provide a user manual, but rather to (1) give a succinct description of the algorithms implemented; (2) highlight features that are not available in existing timing packages; and (3) describe the accuracy of TEMPO2. Full documentation and download instructions for TEMPO2 can be obtained from our web site.[2] Details of the algorithms used in TEMPO2 in order to achieve accuracies of 1 ns will be presented in Paper II of this series (Edwards, Hobbs & Manchester, in preparation). Methods to simulate the effects of gravitational waves on pulsar-timing data and utilities to place limits on the existence of a gravitational wave background will be described in Paper III.

In Section 2, we describe real and simulated pulse arrival times used for testing and demonstrating the various features of TEMPO2. Section 3 provides a description of the conversion between site arrival times to arrival times in the pulsar frame through the use of clock correction files, propagation delays and a planetary ephemeris. The fitting algorithms implemented in TEMPO2 for single data sets are described in Section 4. Section 5 describes analysis methods for the fitted parameters and their uncertainties, and Section 6 contains information on TEMPO2 routines to study the resulting timing residuals. TEMPO2 provides a predictive facility which is described in Section 7.

2 REAL AND SIMULATED PULSE ARRIVAL TIMES

The TEMPO2 software is based around (1) an 'engine' that calculates the barycentric arrival times, forms the timing residuals and carries out the weighted least-squares fit; and (2) 'plug-ins' that add to the functionality of TEMPO2 and allow the results to be analysed and presented in a user-friendly form. For instance, a plug-in is available to plot the timing residuals of multiple pulsars simultaneously, another to determine the power spectrum of the residuals and another to graph the clock corrections that TEMPO2 is applying to the measured arrival times. A full listing of the currently available plug-ins is provided in Appendix A.

It is now common to combine TOAs obtained at different observatories with different back-end systems and receivers. These almost invariably give rise to a constant offset or 'jump', between each set of TOAs. TEMPO2 can fit for such jumps between observations at different telescopes, with different observing frequencies or back-end systems, between a range of dates, or on any other given parameter. This is made possible by a new free format for the measured pulse-arrival times. This free format allows additional flags providing user-definable parameters such as the back-end system, the observation length or the observation bandwidth. Using the graphical plug-in features, it is also possible to plot the pre- and post-fit timing residuals versus time or other parameters such as the observation length, parallactic angle or attenuation settings.

It is essential to test the algorithms implemented within TEMPO2 with precise TOAs. We have selected three pulsars, listed in Table 1 that have been observed for the Parkes Pulsar Timing Array (PPTA) project[3] which aims to detect gravitational waves by looking for correlated signatures in the timing residuals of multiple pulsars (Jenet et al. 2005). Timing residuals for these pulsars are shown in Fig. 1. PSRs J0437−4715 and J1909−3744 provide high-quality timing observations at the sub-500 ns level. PSR J1022+1001 has an ecliptic latitude of $-0.^{\circ}06$ and, hence, the TOAs are affected by Solar system dispersion and Shapiro delays. Full details of the project and observing details will be described in a later paper.

Table 1. A selection of the pulsars observed in the PPTA project. We list the pulsars' names, pulse frequencies (ν), observing spans, numbers of TOAs ($N_{\rm TOA}$), observing frequencies (f) and the post-fit rms residuals (rms).

PSR	ν (Hz)	Span (d)	$N_{\rm TOA}$	f (MHz)	rms (μs)
J0437−4715	173.6879	761	6382	1340	0.49
J1022+1001	60.7794	600	142	3100/1400/685	3.7
J1909−3744	339.3157	542	56	3100	0.35

For more detailed tests we use a TEMPO2 plug-in capable of simulating pulsar-timing residuals in the presence of red noise or with glitch events (see Fig. 2). These TOAs are determined by repeatedly forming the pulsar-timing residuals and then subtracting these residuals from the TOAs until the TOAs exactly match the timing model provided. The simulated residuals are then output after the addition of 'white' (Gaussian) and/or 'red' noise (modelled by summing many sinusoids with random phase, but with amplitudes given by the requested power-law spectrum).

3 FORMING THE PULSE EMISSION TIME

The timing procedure starts by converting the measured topocentric TOAs to the pulse emission time in the pulsar frame ignoring the frequency-independent propagation delay from the pulsar to the SSB. Full details of this transformation, its accuracy and differences relative to TEMPO1 will be described in Paper II. Here we summarize the transformation as

$$\Delta t = \Delta_{\rm C} + \Delta_{\rm A} + \Delta_{\rm E_\odot} + \Delta_{\rm R_\odot} + \Delta_{\rm S_\odot} - D/f^2 + \Delta_{\rm VP} + \Delta_{\rm B}, \quad (1)$$

where $\Delta_{\rm C}$ contains various clock corrections (see Section 3.1), $\Delta_{\rm A}$ the atmospheric propagation delays (Section 3.2), $\Delta_{\rm E_\odot}$ the Solar system Einstein delay (Section 3.3), $\Delta_{\rm R_\odot}$ the Solar system Roemer delay (Section 3.4), $\Delta_{\rm S_\odot}$ the Solar system Shapiro delay (Section 3.4.1), D/f^2 models the dispersive component of the light travel time (Section 3.5), $\Delta_{\rm vp}$ describes the excess vacuum propagation delay due to secular motion (Section 3.6) and $\Delta_{\rm B}$ contains terms that describe any orbital motion (Section 5.3). In Table 2, we list various effects that must be taken into account when forming barycentric arrival times from the observed TOAs. The table also provides a typical value or range for the magnitude of each effect and whether or not it is included in TEMPO1.

3.1 Clock corrections

The TOAs provided to TEMPO2 are recorded against local observatory clocks. Such clocks are typically derived from a precision frequency standard with good short-term stability, such as a hydrogen maser. On longer time-scales (months to years) these clocks deviate significantly from uniformity and are therefore unsuitable for precision pulsar timing. However, it is generally possible to remove these errors down to the precision provided by the best available

[2] http://www.atnf.csiro.au/research/pulsar/tempo2.
[3] http://www.atnf.csiro.au/research/pulsar/ppta.

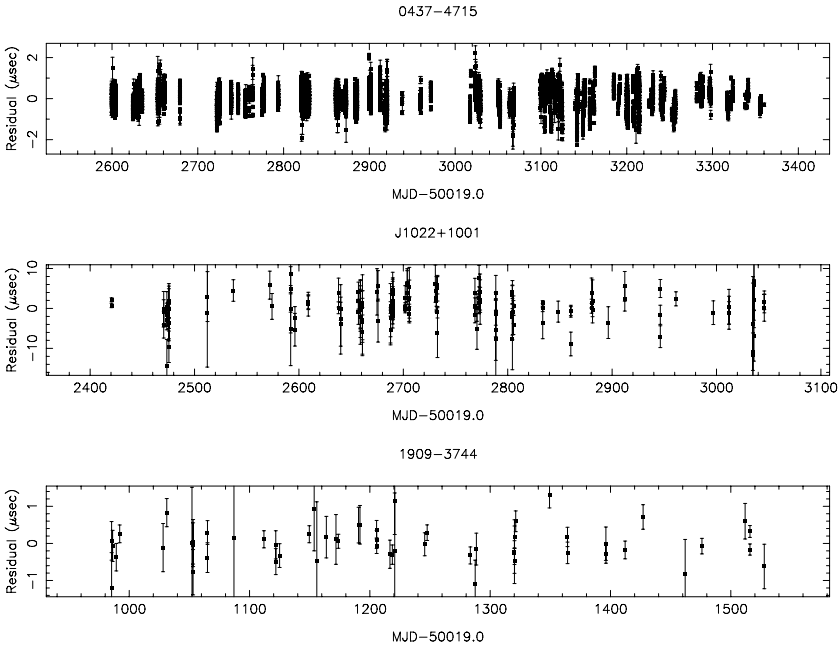

Figure 1. The timing residuals for PSRs J0437−4715, J1022+1001 and J1909−3744 observed as part of the PPTA project. This figure was produced using the SPLK interface to TEMPO2.

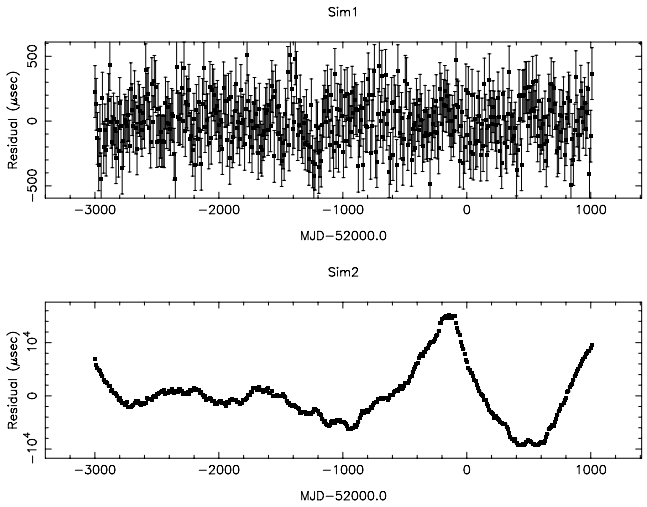

Figure 2. TEMPO2 simulations of 'white' (upper panel) and 'red' (lower panel) timing residuals. The lower panel contains both red timing noise simulated using a steep power-law spectrum and a small glitch event at MJD 519 00. This figure was produced using the FAKE and SPLK interfaces to TEMPO2.

Table 2. Corrections and their typical sizes for phenomena included in TEMPO2.

Correction	Typical value/range	TEMPO1
Observatory clock to TT	1 μs	Y
Hydrostatic tropospheric delay	10 ns	N
Zenith wet delay	1.5 ns	N
IAU precession/nutation	∼5 ns	N[a]
Polar motion	60 ns	N
ΔUT1	1 μs	Y
Einstein delay	1.6 ms	Y
Roemer delay	500 s	Y
Shapiro delay due to Sun	112 μs	Y
Shapiro delay due to Venus	0.5 ns	N
Shapiro delay due to Jupiter	180 ns	N
Shapiro delay due to Saturn	58 ns	N
Shapiro delay due to Uranus	10 ns	N
Shapiro delay due to Neptune	12 ns	N
Second-order Solar Shapiro delay	9 ns	N
Interplanetary medium dispersion delay	100 ns[b]	Y
ISM dispersion delay	∼1 s[b]	Y

[a]Earlier precession/nutation model implemented.
[b]Observing frequency- and pulsar-dependent, typical value for 1400 MHz listed.

terrestrial time-scale through the application of corrections derived from monitoring the offsets between pairs of clocks. For example, the PPTA pulsars are observed at the Parkes Observatory where the offset between the observatory 1 pulse-per-second signal (derived from a hydrogen maser) is compared both to the clock signal broadcast by Global Positioning System (GPS) satellites and by common-view GPS monitoring to the Australian national time-scale Universal Coordinated Time (UCT) (AUS), maintained by the National Measurement Institute. The Bureau International des Poids et Mesures (BIPM) in turn publishes a monthly bulletin (Circular T) tabulating offsets between various clock pairs. Using Circular T, measurements can be referred from an intermediate clock [e.g. UCT (AUS) or GPS time] to UCT. UCT is a time-scale formed through the weighting of data from an ensemble of atomic clocks from around the world. This in turn is related to Temps Atomique International (TAI) by an integer number of 'leap' seconds, which are inserted to maintain approximate synchrony between UCT and the irregular rotation of the Earth (these are announced in Bulletin C of the International Earth Rotation Service). TAI is the most stable long-term time-scale available in near real-time.

The ultimate aim of the clock correction process is to transform measurements into the Geocentric Celestial Reference

System (GCRS), for which the coordinate time is denoted by GCT, expressed in units of the SI second. Owing to their gravitational and rotational energy, terrestrial atomic clocks made to approximate the SI second do not run at the same rate as GCT. Instead, these clocks are used to define realizations of a time-scale known as Terrestrial Time (TT), which differs from GCT by a constant rate in such a way that its unit corresponds to the SI second on the surface of the geoid. One possible realization of TT is obtained directly from TAI:

$$\mathrm{TT\,(TAI)} = \mathrm{TAI} + 32.184\ \mathrm{s}, \quad (2)$$

however, TAI has instabilities and inaccuracies for which corrections frequently become available at a later date. The best available stability is currently provided by the retroactive time-scales published by the BIPM (Guinot 1988; Petit 2003), the most recent of which is denoted by TT (BIPM04).

The TEMPO2 framework for handling clock corrections was designed with maximum flexibility in mind, with the possibility of processing data sets with a heterogeneous collection of different observatories, clocks, and clock correction paths. The scheme is based around a data base of ASCII files tabulating the offsets between named pairs of clocks. Given the name of the clock against which a TOA is measured, and the name of the realization of TT to which it should be transformed, corrections can be applied based on a manually or automatically determined sequence derived from linear interpolation of values from files found in the database. Step changes such as leap seconds are also possible. An ancillary suite of programs allows for the production of TEMPO2 format files from external data sources such as Circular T, and provides capabilities for averaging, resampling and various analytic procedures for assessing the quality of data present.

3.2 Atmospheric propagation delays

The group velocity of radio waves in the atmosphere differs from the vacuum speed of light. Refractivity is induced both by the ionized fraction of the atmosphere (mainly in the ionosphere) and the neutral fraction (mainly in the troposphere). The tropospheric propagation delay can be separated into the so-called 'hydrostatic' and 'wet' components (see Paper II). For the highest timing precision, it is possible to provide TEMPO2 with a tabulated list of surface atmospheric pressure measured at an observatory for the calculation of the hydrostatic delay which will be of the order of 10 ns. If atmospheric pressure data are unavailable, then TEMPO2 can, if required, use a canonical value of one standard atmosphere. This assumption results in errors of the order of 1.5 ns. In Fig. 3, we show computed hydrostatic tropospheric delays for simulated TOAs for PSR J1022+1001, assuming a constant surface atmospheric pressure and a ± 5-h hour-angle range. Diurnal variations arise due to the dependence of atmospheric path length on source elevation (in the simulated observations the elevation varies from 6° to 46°).

The wet component of the tropospheric propagation delay (the zenith wet delay, ZWD) is highly variable and cannot be predicted accurately. If no tabulated ZWD information is available, the effect is neglected, otherwise tabulated data may be used. With a typical excess zenith path length of 100–400 mm, error is incurred at the level of approximately 1.5 ns.

3.3 Einstein delay

The Einstein delay (Damour & Deruelle 1986) quantifies the change in arrival times due to variations in clocks at the observatory and the SSB due to changes in the gravitational potential of the Earth and the Earth's motion. The IAU resolution A4 (1991) recommends the use of barycentric coordinate time (BCT) which differs from TT both in mean rate and in periodic and quasi-periodic terms. By default, this is the coordinate time in which arrival times are specified in TEMPO2. Prior to the definition of BCT, the recommended barycentric coordinate time was barycentric dynamical time (BDT) which was implemented in TEMPO1. In addition to being physically unrealizable (Standish 1998), BDT values are not physical coordinate times, but rather values of a variable related to time by a dimensionless scale factor (Klioner 2005). If these values are taken as barycentric coordinate times of arrival, as has been a common practice in the past, then the scaling factor is effectively transferred from the value to the units. Therefore, although site arrival times are referred to TT, which is defined in terms of the SI second, BDT barycentric arrival 'time' intervals, and in fact, the numerical values of all parameters inferred with pulsar timing on the basis of BDT TOAs are effectively measured in units that differ subtly from their SI counterparts.

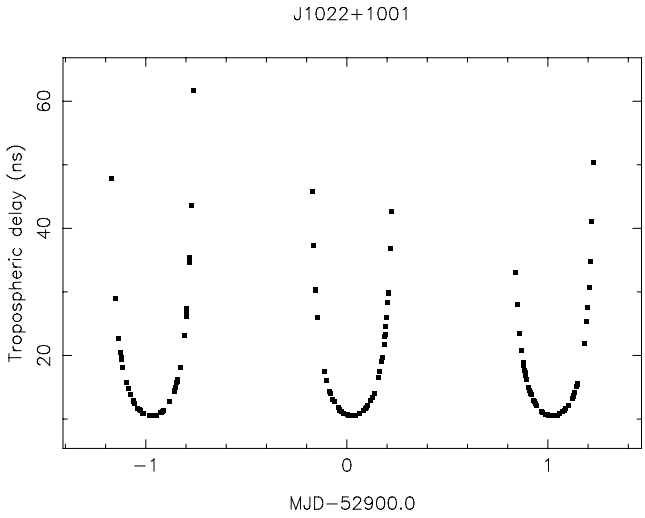

Figure 3. The computed hydrostatic tropospheric delay for simulated pulse times of arrival, assuming a constant surface atmospheric pressure.

As a result, all catalogued parameters measured using BDT TOAs (e.g. those from TEMPO1) must be multiplied by

$$K = 1 + (1.550\,519\,791\,54 \times 10^{-8} \pm 3 \times 10^{-17}) \quad (3)$$

(Irwin & Fukushima 1999). This can be a large effect and timing models created using TEMPO1 need to be modified before being used by TEMPO2. The nth frequency-derivative scales as $K^{-(n+1)}$ and the orbital period and semimajor axis all scale as K. The epochs of periastron, period, position and DM all scale as K in their offset from the common epoch of Modified Julian Day (MJD) 431 44.000 3725 (Irwin & Fukushima 1999). For instance, the modification in pulse frequency produces a slope of $0.5\,\mathrm{s\,yr^{-1}}$ in the timing residuals which, for millisecond pulsars, will lead to phase coherence being lost over even short data spans. Using the TRANSFORM plug-in, TEMPO2 provides an interface that can be used to convert old parameters into the new system. We also emphasize that, because of the significant differences between the BDT and BCT, for all published timing models the coordinate frame used must be clearly specified.

3.4 Roemer delay

The Roemer delay is the vacuum light travel time between the pulse arriving at the observatory and the equivalent arrival time at the SSB.

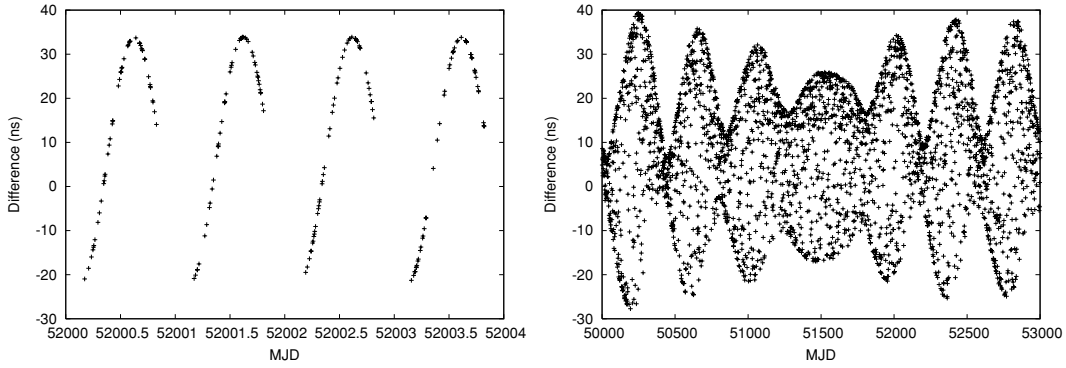

Figure 4. Differences in the Solar system Roemer delay computed using current IAU precession–nutation models and including polar motion, versus the algorithm of TEMPO1 for simulated TOAs from PSR J1022+1001. The diurnal timing term is shown in the left-hand plot which is modulated by the yearly and 435-d periodicities of the polar motion (right-hand plot) which, in turn, beat with a ∼6-yr period.

In TEMPO2 this is calculated by determining the time-delay between a pulse arriving at the observatory and at the Earth's centre and, with the aid of a Solar system ephemeris, from the Earth's centre to the SSB.

The coordinates of the pulsar are known, either from telescope pointing, interferometry or pulsar timing, and are normally measured in the International Celestial Reference System (ICRS).[4] The required transformation between the ICRS and the International Terrestrial Reference Frame (ITRF), within which observatory positions are determined, depends on precession, nutation, polar motion and the Earth rotation. The worst-case timing offset resulting from a positional error of $\Delta\theta$ is given by $\Delta\theta R_\oplus/c$, that is,

$$\frac{\Delta t}{1\ \mathrm{ns}} \simeq \frac{\Delta\theta}{9.7\ \mathrm{mas}}. \quad (4)$$

Through its omission of polar motion amounting up to ±300 mas (corresponding to ±30 ns) and also through the use of the IAU 1976 precession (Lieske et al. 1977) and IAU 1980 nutation (Seiber 1982) models which are in error at the 50 mas (5 ns) level, the TEMPO1 software introduces errors in the timing model that are significant at contemporary levels of timing precision. In TEMPO2, polar motion is corrected using the values published in the C04 series of Earth Orientation Parameters (EOP) of the International Earth Rotation Service (IERS). The IERS also provides the difference between the observed precession and nutation and that predicted by the IAU 1976 and 1980 models. However, following the recommendations of IAU Resolutions adopted at the 24th General Assembly, we adopt the IAU 2000 precession–nutation model which provides sufficiently accurate predictions. Specifically, TEMPO2 uses the truncated 2000B model (McCarthy & Luzum 2003) which is accurate to 1 mas (0.1 ns). Fig. 4 shows the differences between the Solar system Roemer delay computed using TEMPO1 and TEMPO2 using simulated observations of PSR J1022+1001. Differences in the model (mainly due to polar motion) introduce an error in the assumed observatory position, which appears as a diurnal timing term which is modulated by the yearly and 435-d periodicities of the polar motion.

[4] In the case of positions obtained by pulsar timing, this is only true if the reference frame of the Solar system ephemeris is tied to the ICRS, for example, by using the DE405 planetary ephemeris. The DE200 ephemeris is offset from the ICRS by ∼14 mas (Folkner et al. 1994), yielding a potentially significant error in the transfer to the geocentre if such a position is used; see Paper II.

The third component in the transformation of the pulsar position to the ITRF is the Earth rotation angle which is a linear function of the time-scale known as UT1. This is computed by TEMPO2 using the offset between UTC and UT1 as provided in the C04 EOP series.

The choice of Solar system ephemeris for determining the position of the SSB with respect to the Earth can have significant effects on the calculated timing residuals. Until recently the Jet Propulsion Laboratory (JPL) DE200 model (Standish 1990), which is based on the dynamical equator and equinox of J2000, was the most widely used. More recently, the JPL DE405 model has been developed[5] which, in contrast to the DE200 model, is aligned with the ICRS (Standish 1998). The DE405 model includes the planets, the Earth's Moon and 300 asteroids. In the left-hand panel of Fig. 5, we plot the difference between residuals obtained using the DE405 and DE200 models after the subtraction of an annual sinusoid (corresponding to a position error) and quadratic term (corresponding to the spin-frequency and its first derivative) for simulated observations of PSR J1909−3744. The right-hand panel contains the timing residuals after fitting for five frequency-derivative terms, the orbital period, epoch of periastron, proper motion and parallax. The use of the DE200 model leads to an incorrect measurement of the proper motion in right ascension (RA) by $-0.2775(3)\ \mathrm{mas\ yr^{-1}}$, in declination (Dec.) by $-0.037(1)\ \mathrm{mas\ yr^{-1}}$ and parallax by $-0.045(5)$ mas over this simulated, regularly sampled data span of 14 yr. Splaver et al. (2005) also reported significant deviations between residuals for PSR J1022+1001 using these Solar system ephemerides during the years 1998–99 which they explained by the new ephemeris incorporating improved measurements of the outer planet masses. Although TEMPO2 can access any of the JPL planetary ephemerides, we currently recommend that the DE405 model be used for any high-precision analysis of pulse-arrival times.

3.4.1 Shapiro delay

To make an accurate determination of the arrival time at the barycentre, it is also necessary to include the Shapiro delay due to Solar system objects (most notably the Sun) which accounts for the time-delay caused by the passage of the pulse through large gravitational fields (Shapiro 1964). Table 2 shows the maximum variation in Shapiro delay for a selection of Solar system bodies. TEMPO2 includes all bodies for which the maximum variation is greater than

[5] ftp://ssd.jpl.nasa.gov/pub/eph/export/DE405/de405.iom/.

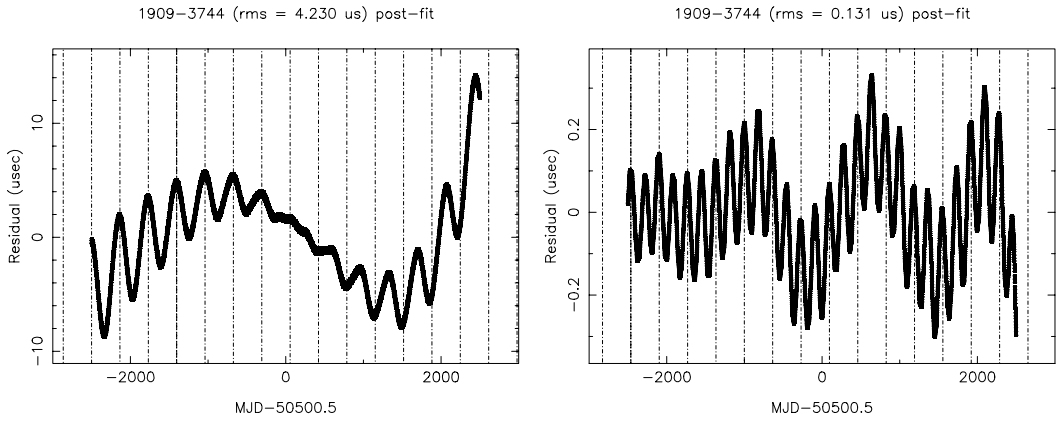

Figure 5. Comparison between timing residuals obtained using the DE200 Solar system ephemeris and the DE405 ephemeris. In the left-hand plot, terms corresponding to a pulsar position error, spin-frequency and its first derivative have been subtracted. In the right-hand plot, terms corresponding to the above and higher frequency derivatives, orbital period, epoch of periastron, proper motion and parallax have also been removed. The vertical lines are spaced at 1-yr intervals. These plots were created using the PLK plug-in for TEMPO2.

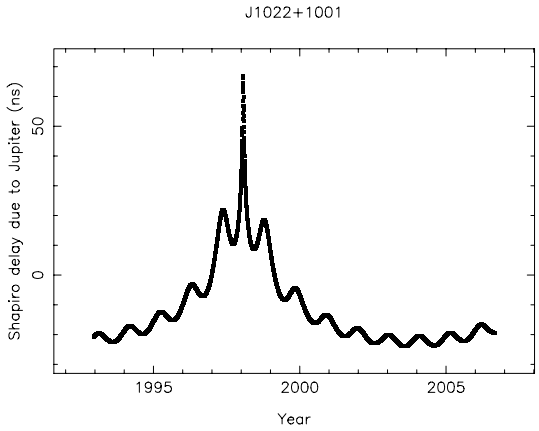

Figure 6. The additional time-delay from the Shapiro delay due to Jupiter for PSR J1022+1001.

0.1 ns. Fig. 6 shows the variations in the Shapiro delay due to Jupiter for PSR J1022+1001.[6] The effect of the Shapiro delay due to the Sun can be clearly seen in the observations of PSR J1022+1001 which has an ecliptic latitude of $-0\overset{\circ}{.}06$. In Fig. 7(a), we plot the pulse timing residuals after fitting for the pulsar's parameters and the Solar system Shapiro delay. Fig. 7(b) shows the resulting timing residuals if the best-fitting parameters are used, but the Solar system Shapiro delay is not calculated when forming the barycentric arrival times. On MJD 53143, this pulsar passed within 5° of Jupiter. However, the additional Shapiro delay due to Jupiter is not detectable with our current data.

3.5 Frequency-dependent parameters

TEMPO2 provides the ability to fit for delays which are dependent on the observing frequency; see Table 3. For instance, dispersion-measure (DM) delays are $\propto f^{-2}$ whereas delays caused by refractive and diffractive effects are $\propto f^{-4}$ (e.g. Foster & Cordes 1990).

[6] The Shapiro delay as characterized by Damour & Dereulle (1986) can be negative. However, as the zeroth-order time of arrival of the pulses is arbitrary, a constant offset can be added to the Shapiro delay calculation.

TEMPO2 allows fitting for a parameter that is $\propto f^{-\zeta}$ where ζ is defined by the user and is not restricted to integral values. We emphasize that in order to obtain absolute values for these frequency-dependent terms it is necessary to obtain TOAs using aligned standard templates. In practice, true absolute alignment is impossible because of profile shape evolution with frequency, so frequency-dependent parameters are always relative at some level.

Although DM values are commonly published, the directly measurable parameter from pulsar-timing observations is D, the dispersion constant, where

$$\mathrm{DM} = D/k_{\mathrm{D}}. \tag{5}$$

If the effect of ions and magnetic fields in the ISM are ignored, then

$$k_{\mathrm{D}} = \frac{e^2}{\pi^2 m_e c}. \tag{6}$$

However, ions and magnetic fields introduce a rather uncertain correction of the order of a part in 10^5 (Spitzer 1962), comparable to the uncertainty in some measured DM values (e.g. Phillips & Wolszczan 1992). Consequently, both TEMPO1 and TEMPO2 adopt a value of $k_{\mathrm{D}} \equiv 2.410 \times 10^{-16}\,\mathrm{cm^{-3}\,pc\,s}$ (Manchester & Taylor 1977). It is also possible, in TEMPO2, to set $k_{\mathrm{D}} = 1$ in order to measure the dispersion constant.

Another dispersive component occurs in the Solar system. The interplanetary medium is dominated by the Solar wind and is approximated in TEMPO2 with the electron density decreasing as an inverse square law from the centre of the Sun (full details are provided in Paper II) with n_0 being the electron density at the Earth. TEMPO1 uses $n_0 = 9.961\,\mathrm{cm^{-3}}$. However, by default, TEMPO2 uses a value of $n_0 = 4\,\mathrm{cm^{-3}}$ which is more consistent with recent measurements (Issautier et al. 1998). Fig. 8 shows the extra time-delay added by TEMPO2 for simulated observations of PSR J1022+1001. As discussed in Paper II, this estimation of the extra time-delay is poor as the true electron density can vary dramatically. We therefore recommend that, for high-precision timing, TEMPO2 be provided with multiple frequency observations which allow the determination of the actual DM for each observation.

As an example, the PPTA uses a dual-band receiver at 10 and 50 cm. The DM at any instant can therefore be measured to a precision of up to $1 \times 10^{-4}\,\mathrm{cm^{-3}\,pc}$ if the difference between observations at the two frequencies can be measured to 1 μs. TEMPO2 can be run in a mode where simultaneous (or contemporaneous) observations

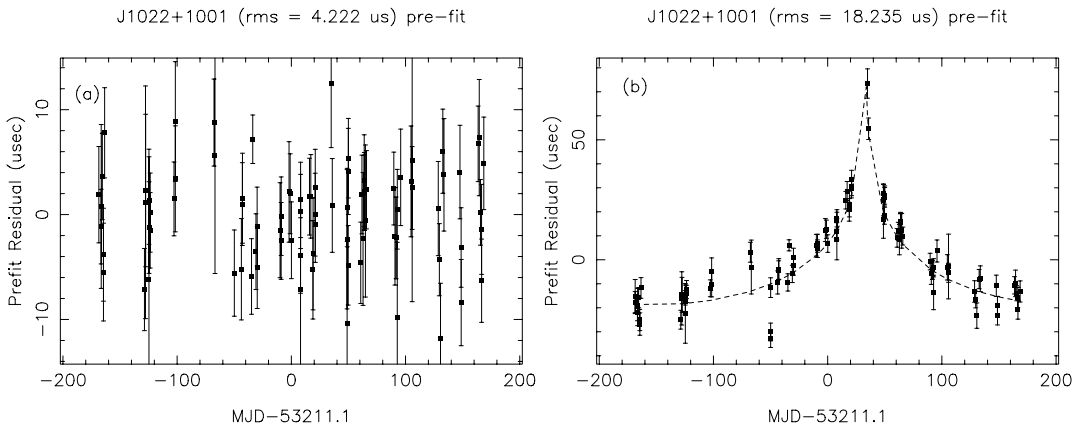

Figure 7. The timing residuals, in μs, for PSR J1022+1001, (a) after fitting for the pulsar's parameters and (b) without removal of the Solar system Shapiro delay. This plot was created using the PLK plug-in for TEMPO2 (note, the original PLK plotting package incorrectly plotted the uncertainties on the residuals; the errors were a factor of 2 too small).

Table 3. TEMPO2 parameters relevant to frequency-dependent offsets.

Parameter	Description	Symbol
DM, DM1 ...	The dispersion measure and its derivatives	DM, $\dot{\text{DM}}$ ...
DMEPOCH	The epoch of the dispersion measure (MJD)	t_{D}
FDDI	Index for frequency-dependent delay	ζ
FDDC	Scale for frequency-dependent delay	k_{f}

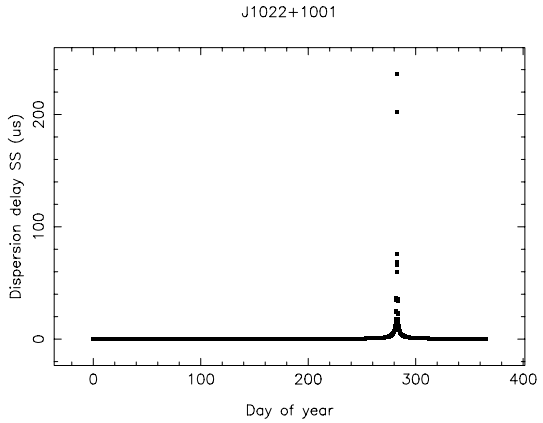

Figure 8. The extra time-delay automatically added by TEMPO2 to model the interplanetary medium for PSR J1022+1001 at an observing frequency of 1400 MHz. This figure was produced using the FAKE and DELAYS plug-ins for TEMPO2.

at multiple frequencies are used to determine the current DM and to use that value in subsequent calculations. For times when there are no multifrequency observations available, the DM can be estimated from a polynomial fit to measured DM values before and after the observation.

3.6 Shklovskii effect and radial motion

Pulsar-timing measurements are affected by the secular motion of the pulsar relative the SSB. In the past the secular terms involving this motion have been omitted from timing models, because they can be absorbed in alterations of other parameters. The four largest effects are the radial velocity (affecting most spin and binary parameters; Damour & Deruelle 1986), the Shklovskii effect and radial acceleration (affecting the spin and orbital period derivatives; Shklovskii 1970; Damour & Taylor 1991) and the mixing of radial velocity into the Shklovskii term (affecting the spin period second derivative; van Straten 2003). In contrast to TEMPO1, TEMPO2 takes the approach that these terms can be included in the timing model as long as steps are taken to ensure the model is sufficiently constrained. In this way, one may take into account what is known about the secular motion and distance (via e.g. its appearance in the annual proper motion and parallax terms) to provide correct measurements of the spin and orbital parameters, rather than measuring incorrect values and attempting to correct them post facto (e.g. Damour & Taylor 1991). Conversely, if one may safely assume that one of the affected spin or orbital parameters is zero, it may be held fixed at this value in order to obtain a direct measurement of the distance or velocity, rather than measuring incorrect spin and orbital parameter values and using these to infer the motion and distance indirectly (e.g. Bell & Bailes 1996; van der Swaluw 2003).

4 FITTING ROUTINES

TEMPO2 uses the derived time of emission and a given timing model to form the ith pre-fit timing residual:

$$R_i = \frac{\phi_i - N_i}{\nu}, \tag{7}$$

where ϕ_i describes the time-evolution of the pulse phase based on the model pulse frequency (ν) and its derivatives in addition to any glitch parameters. N_i is the nearest integer to ϕ_i. Paper II contains details for calculating ϕ_i.

Terms corresponding to offsets in model parameters are fitted to these residuals in order to improve the measurement of these parameters. By default, the entire procedure is repeated using the post-fit timing model in order to produce accurate post-fit barycentric arrival times and residuals. This is in contrast to TEMPO1 which only obtains the barycentric arrival times once and predicts the expected post-fit timing residuals. This entire process often needs to be iterated until convergence is reached as the offsets made to model parameters are based on a linearized approximation to the effects on the timing model (e.g. Damour & Deruelle 1986).

The fitting routines in TEMPO2 are based on a linear singular-value decomposition, weighted least-squares algorithm (e.g. Press et al.

Table 4. Comparison between standard least-squares (LS) parameters and uncertainties with those obtained using a bootstrapping (BS) technique for PSR J1909−3744.

Parameter	Value ($V_{\rm LS}$)	Error ($E_{\rm LS}$)	Value ($V_{\rm BS}$)	Error ($E_{\rm BS}$)	$E_{\rm BS}/E_{\rm LS}$
RA (rad)	5.016 908 214 879	3.5×10^{-11}	5.016 908 214 880	4.3×10^{-11}	1.2
Dec. (rad)	−0.658 639 870 98	1.4×10^{-10}	−0.658 639 871 00	2.1×10^{-10}	1.5
Pulse frequency (Hz)	339.315 687 629 26	1.9×10^{-12}	339.315 687 629 26	2.4×10^{-12}	1.3
Frequency derivative (s^{-2})	$-1.614\,873 \times 10^{-15}$	2.4×10^{-20}	$-1.614\,878 \times 10^{-15}$	2.9×10^{-20}	1.2
Orbital period (d)	1.533 449 474 188	1.1×10^{-11}	1.533 449 474 191	1.4×10^{-11}	1.3
Projected semimajor axis (lt-s)	1.897 991 295	9.9×10^{-9}	1.897 991 295	1.2×10^{-8}	1.2
Epoch of periastron (MJD)	520 53.452	0.021	520 53.443	0.020	0.95
Eccentricity	1.186×10^{-7}	9.5×10^{-9}	1.187×10^{-7}	9.6×10^{-9}	1.0

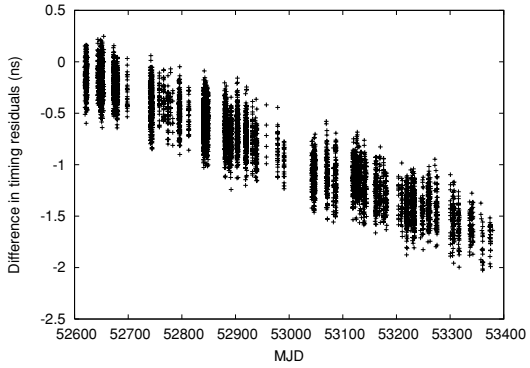

Figure 9. Comparison between TEMPO1 and TEMPO2 timing residuals for the PSR J0437−4715 observations when TEMPO2 is emulating TEMPO1. No clock corrections were applied to the TOAs.

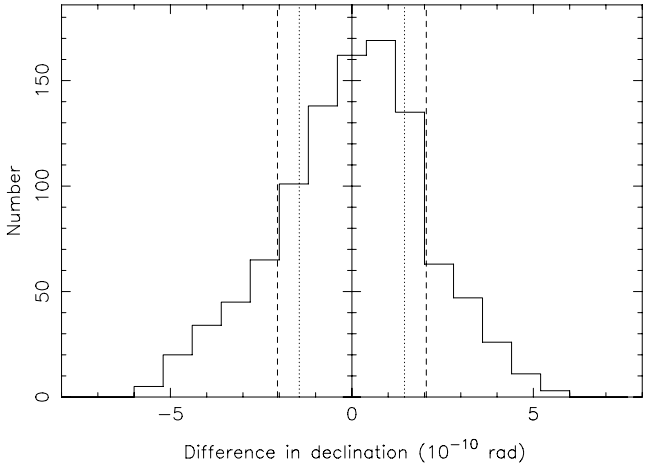

Figure 10. Histogram of the Dec. parameter obtained using the bootstrap technique for PSR J1909−3744. The dashed lines indicate the 1σ uncertainties obtained using this method and the dotted lines give the 1σ uncertainties measured using the standard least-squares-fitting routine.

1992)[7] where

$$\chi^2 = \sum_{i=1}^{N} \left(\frac{R_i}{\sigma_i} \right)^2 \quad (8)$$

is minimized. N is the number of observations and $\sigma_i = 1$ for unweighted fits or set to the TOA uncertainty for the ith observation for a standard χ^2-minimization. If specified as Modified Julian dates, measured TOAs need to be accurate to better than 19 significant figures for 1-ns timing precision and spin frequencies are now routinely measured to 16 significant figures. In TEMPO2, all parameters are stored and all calculations are carried out with 'long double' precision that typically provides 12 bytes of storage (allowing 18 significant digits) on PC-based systems and 16 bytes (33 significant digits) on most other systems. In Fig. 9, we plot the difference between the pre-fit timing residuals for PSR J0437−4715 obtained using TEMPO1 and TEMPO2. The observed trend that covers ∼2 ns over 2.1 yr of observing is due to TEMPO1 not storing the pulse frequency with enough significant figures and will lead to TEMPO1 introducing systematic effects in the timing residuals over long time-spans.

It is also useful to compare the formal uncertainties described above with those obtained using a 'bootstrapping' method (see e.g. Wall & Jenkins 2003) which can produce more realistic parameter values and uncertainties when significant correlations between parameters are present. The bootstrapping method implemented in TEMPO2 estimates the uncertainty on a parameter by (1) randomly selecting observations to produce a new data set of the same length as the original (the observations are selected with replacement; that is, in the new data set some of the original observations will be omitted while others will be replicated); (2) recalculating the parameter; and (3) repeating as many times as possible.[8] The distribution of these parameters provides an estimate of the uncertainty (obtained from the standard deviation of the distribution) on the value of the parameter (taken as the mean of the distribution). In Table 4, we compare the values and uncertainties on the fitted parameters using the formal least-squares fitting and the bootstrap technique with 1024 iterations for PSR J1909−3744. For this pulsar, with residuals that are not dominated by timing noise, the measured uncertainties are typically ∼1.2 times larger with the bootstrap technique than with the least-squares method. A histogram of the fitted Dec. is shown in Fig. 10.

Various interfaces exist that allow the user to study the actual fits being applied to the pre-fit timing residuals. For instance, in Fig. 11(a), we plot the components of the fit when improving a pulsar's proper motion and parallax. In Fig. 11(b) we demonstrate

[7] It is possible with plug-in capabilities to use a non-linear fitting algorithm, but this is not necessary for the routines described in this paper; more details will be provided in Paper III.

[8] Note: the bootstrapping method implemented in TEMPO1 does not re-fit for the parameters after randomly selecting observations and is therefore not a true bootstrapping technique.

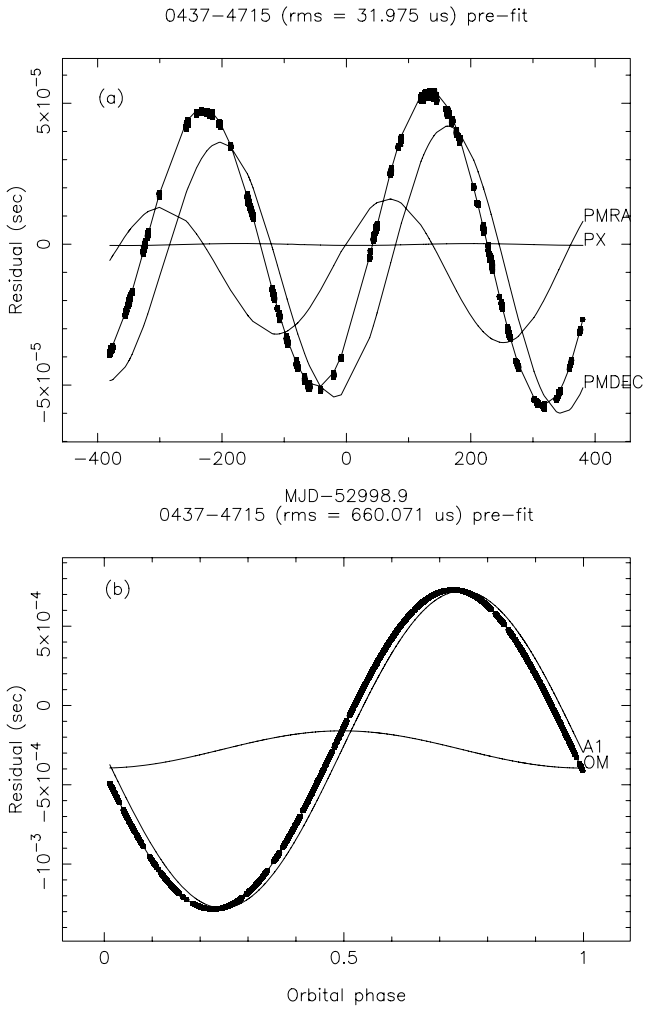

Figure 11. The components of a fit to update a pulsar's (a) proper motion and parallax and (b) longitude of periastron and projected semimajor axis of orbit (assuming that these are the only parameters being updated). The line through the measured residuals indicates the sum of the model components. These plots were created using the PLK plug-in for TEMPO2.

the effects of poorly estimated binary parameters. The TEMPO2 software also provides the ability to fit one or more of the timing model parameters over short adjacent subsets of the data. For example, this allows the user to analyse DM variations (Fig. 12), search for glitch events and to confirm proper motions.

It is often difficult, with sparse observations, to obtain an accurate timing model. This is often solved by making further observations of the pulsar, but with the GORILLA plug-in, TEMPO2 provides an alternative method. For example, 35 observations of PSR J0857−4424 spread over 7 yr were obtained at the Parkes Observatory, but a solution producing phase-connected timing residuals could not be obtained. GORILLA provides a brute-force-fitting technique that obtains the pre-fit timing residuals over many millions of combinations of spin-frequency and its derivative within specified ranges. This method found the correct solution over a 1-yr section of the PSR J0857−4424 data and this fit was extrapolated to phase-connect the entire seven years of observations without the necessity for further observations.

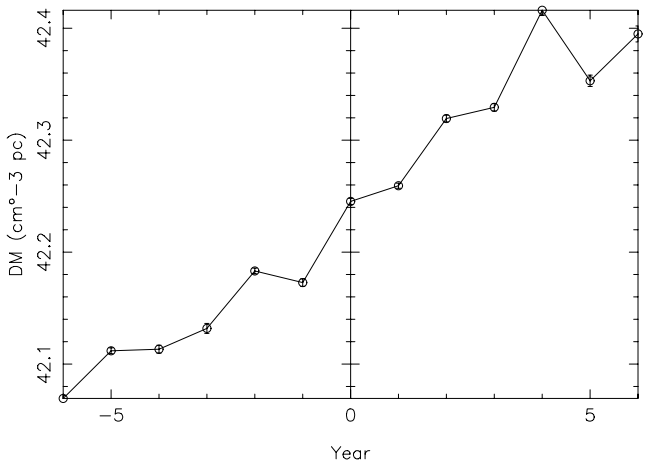

Figure 12. The DM variation for PSR B0458+46 obtained by fitting for DM in 1-yr sections of the Jodrell Bank Observatory data. This plot was produced using the STRIDEFIT plug-in for TEMPO2.

5 THE POST-FIT PARAMETERS AND THEIR ERRORS

5.1 Pulsar spin parameters

TEMPO2 provides the ability to fit for the pulsar's pulse frequency and an arbitrary number of spin-frequency derivatives. The full set of possible spin parameters available are listed in Table 5. Except for the very youngest pulsars, the frequency second and higher derivatives are not believed to represent the secular spin-down of the pulsar, but rather timing irregularities known as timing noise (e.g. Hobbs et al. 2004). For pulsars whose timing residuals are dominated by timing noise, it is not possible to determine accurate positions, proper motions or DMs without 'whitening' the data while fitting the timing model. Traditionally, this whitening procedure has been carried out by fitting multiple spin-frequency derivatives, until the resulting post-fit residuals are free of systematic structure. As described by Hobbs et al. (2004) this whitening technique is limited because (1) only low-frequency timing noise can be modelled without affecting the higher-frequency signatures of position errors and proper motions; and (2) such whitening is limited to polynomials of the order of 12 to prevent floating-point overflows. Hobbs et al. (2004) described a new method, based on the fitting of harmonically related sinusoids, that produces superior results in many cases. This sinusoidal fitting technique has been implemented into TEMPO2. In brief, TEMPO2 obtains from the parameter file a fundamental frequency (ω) and the amplitudes of $n_{\rm H}$ harmonically related sinusoids. If the fundamental frequency is not provided, then it is derived from the observation span ($T_{\rm span}$) as

$$\omega = \frac{2\pi}{T_{\rm span}(1 + 4/n_{\rm H})}. \quad (9)$$

TEMPO2 subsequently subtracts

$$\Delta R = \sum_{k=1}^{n_{\rm H}} a_k \sin(k\omega\Delta t) + b_k \cos(k\omega\Delta t) \quad (10)$$

from the timing residuals where Δt represents the difference between an arrival time in the pulsar reference frame and the specified period epoch. TEMPO2 can also fit for the coefficients a_i and b_i and output these parameters as part of a new timing model. In contrast to the technique described by Hobbs et al. (2004), the default

Table 5. The spin, glitch and whitening parameters included in TEMPO2.

Parameter	Description	Symbol
F0, F1 ...	The pulse frequency and its derivatives	$\nu, \dot{\nu} \ldots$
PEPOCH	The epoch of the pulse-frequency measurement	$t_{\rm P}$
GLEP_k	Glitch epoch (MJD)	$t_{\rm g}$
GLPH_k	Glitch phase increment	$\Delta\,\phi_{\rm g}$
GLF0_k	Glitch permanent pulse frequency increment (Hz)	$\Delta\,\nu_{\rm g}$
GLF1_k	Glitch permanent frequency-derivative increment (s^{-2})	$\Delta\dot{\nu}_{\rm g}$
GLF0D_k	Glitch decaying pulse frequency increment (Hz)	$\Delta\,\nu_{\rm d}$
GLTD_k	Glitch decay time constant (d)	$\tau_{\rm d}$
WAVE_OM	Fundamental frequency of sinusoids for whitening (Hz)	ω
WAVE_k	Amplitude of the sine and cosine terms for the kth sinusoids	a_k, b_k

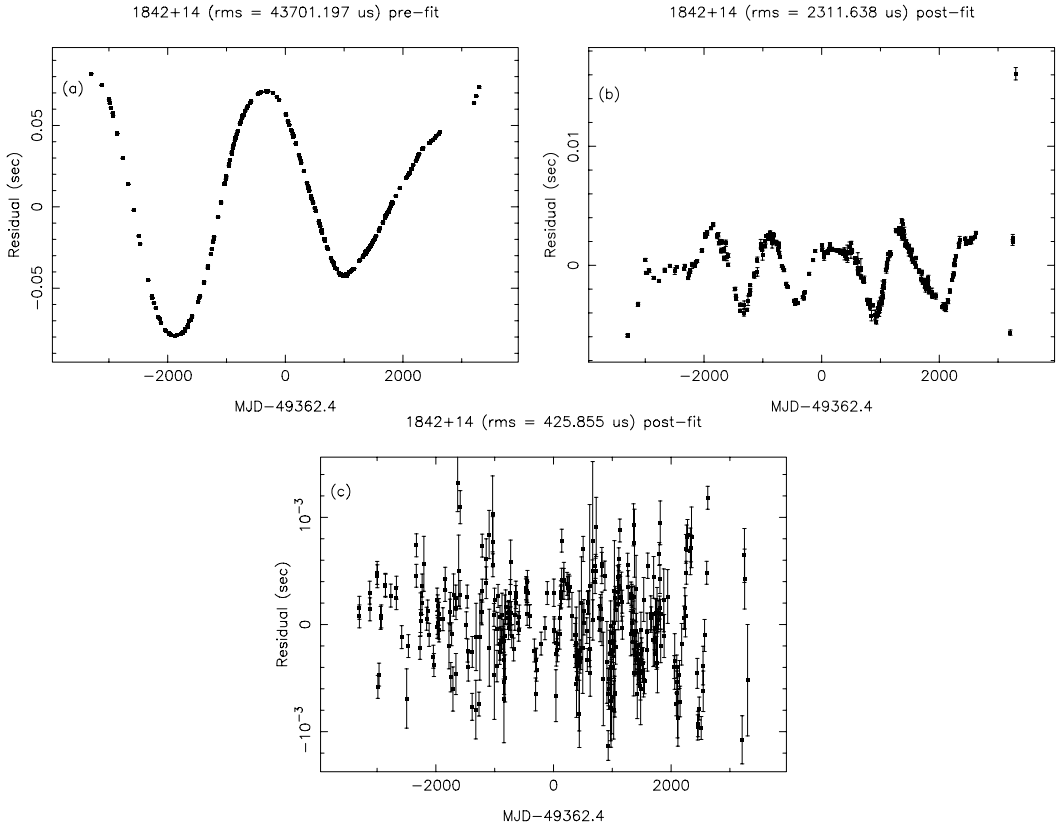

Figure 13. (a) The pre-fit timing residuals for PSR B1842+14 obtained from the Jodrell data archive. (b) Whitening the timing residuals using 11 polynomial coefficients and (c) whitening the timing residuals using sinusoids.

method implemented by TEMPO2 simultaneously fits for the pulsar parameters and for the sinusoids, that is, this is not a pre-whitening technique.

An example of such 'whitening' of the data is shown in Fig. 13. The timing residuals of PSR B1842+14 obtained from the Jodrell Bank data archive are typical of those seen for non-recycled pulsars over many years of observation. They are dominated by quasi-periodic structures that are well modelled using the sinusoidal modelling, but not by high-order polynomial terms.

The pulse frequencies of many young pulsars have been observed to increase suddenly during a glitch event. An individual glitch can be characterized by the epoch of the glitch ($t_{\rm g}$), the phase increment at the glitch ($\Delta\phi_{\rm g}$), a permanent pulse frequency increment ($\Delta\nu_{\rm g}$), a permanent frequency-derivative increment ($\Delta\dot{\nu}_{\rm g}$), a decaying pulse frequency increment ($\Delta\nu_{\rm d}$) and the decay time constant ($\tau_{\rm d}$). The increase in pulse phase due to a glitch event at time $t_{\rm g}$ is given by

$$\phi_{\rm g} = \Delta\phi_{\rm g} + \Delta t\Delta\nu_{\rm g} + \frac{1}{2}\Delta\dot{\nu}_{\rm g}(\Delta t)^2 + \tau_{\rm d}\Delta\nu_{\rm d}(1 - e^{-\Delta t/\tau_{\rm d}}) \qquad (11)$$

where $\Delta t = t - t_{\rm g}$ is the time since the glitch event. TEMPO2 allows the user to fit for an arbitrary number of glitch events in a single data set and provides various plug-ins to aid in their detection.

5.2 Astrometric parameters

TEMPO2 performs computations in the reference frame of the Solar system ephemeris which is approximately equatorial. Since the location of the observatory is specified in the ITRS, and transformed

Table 6. Astrometric parameters included in TEMPO2.

Parameter	Description	Symbol
RA	Right ascension of pulsar (hr min sec)	α
DEC	Declination of pulsar (deg min sec)	δ
ELONG	Ecliptic longitude of pulsar (°)	λ
ELAT	Ecliptic latitude of pulsar (°)	β
PMRA	Proper motion in right ascension (mas yr^{-1})	μ_α
PMDEC	Proper motion in Dec. (mas yr^{-1})	μ_δ
PMELONG	Proper motion in ecliptic longitude (mas yr^{-1})	μ_λ
PMELAT	Proper motion in ecliptic latitude (mas yr^{-1})	μ_β
PX	Parallax (mas)	π
PMRV	Radial proper motion	$\mu_\parallel$
POSEPOCH	Position epoch (MJD)	$t_{\rm pos}$

to the ICRS according to the specifications of the IAU 2000 resolutions, for the best possible accuracy a Solar system ephemeris that is aligned with the ICRS should be used. The JPL DE405 ephemeris is the most recent of the publicly available JPL series and meets this criterion. The TEMPO2 equatorial astrometric parameters ('RA', 'DEC', etc.) strictly refer to the ephemeris frame, which, even in the case of DE405, is only tied to the ICRS within a finite uncertainty. The ICRS itself is measurably offset from both the Fundamental Katalog 5 (FK5; Feissel & Mignard 1998) and the dynamical equator and equinox of J2000.0 (Hilton & Hohenkerk 2004). Seidelmann & Kovalevsky (2002) stated that ICRS coordinates should be denoted by 'RA' and 'Dec.' with no further qualification. Since the coordinates measured using pulsar timing are relative to the coordinate frame of the chosen planetary ephemeris, the latter needs to be specified when quoting fitted positions. Owing to the known offset between J2000.0 and the ICRS, we recommend that the common practice of labelling pulsar-timing coordinates as 'J2000' be discontinued.

TEMPO2 also accepts astrometric parameters specified in the ecliptic frame. For such parameters, TEMPO2 transforms all vectors into the ecliptic coordinate system by rotating about the 'x-axis' by the mean obliquity of the ecliptic, ϵ, at the epoch J2000.0. By default, TEMPO2 uses the current best estimate of the mean obliquity of the ecliptic, $\epsilon_{\rm DE405} = 84\,381.405\,78$ arcsec (Harada & Fukushima 2004). This value is derived from a harmonic decomposition of the DE405 Solar system ephemeris, and applies to the epoch J2000.0. This differs from the earlier estimate of 84 381.412 arcsec used by TEMPO1. Since timing pulsar positions are largely constrained by the Solar system Roemer delay, error ellipses tend to be aligned with ecliptic latitude or longitude, making this basis a convenient choice when one coordinate is constrained more strongly than the other. For instance, fitting for the proper motion in equatorial coordinates with the PSR J1022+1001 data set discussed in Section 2 gives a proper motion in RA $\mu_\alpha = -148(55)$ mas yr^{-1} and in Dec. of $\mu_\delta = -335(143)$ mas yr^{-1} and the astrometric parameters are highly covariant in the fit. Fitting using ecliptic coordinates provides a precise measurement of the proper motion in ecliptic longitude $\mu_\lambda = -16.1(2)$ mas yr^{-1} which can be used in one-dimensional studies of pulsar velocities (e.g. Hobbs et al. 2005) and a much poorer determination in ecliptic latitude $\mu_\beta = -307(152)$ mas yr^{-1}. A full list of the astrometric parameters that can be used by TEMPO2 is listed in Table 6.

5.3 Binary parameters

For pulsars in binary systems, TEMPO2 includes terms that describe the pulsar's orbital motion. Various timing models are available. A full mathematical description of these models and their implementation in TEMPO2 is provided in Paper II. Here, we provide a summary.

The main binary model implemented in TEMPO2 is referred to as the 'T2' model and is based on the Damour & Deruelle (1986) model ('DD') implemented in TEMPO1. In contrast to the 'DD' model which is designed for a pulsar and a single companion, the new 'T2' model allows multiple binary companions. Various other models were available to TEMPO1 and can be emulated using the 'T2' model. For instance, the 'DD' model is more general than the earlier Blandford & Teukolsky (1976) model ('BT'). By making various simplifying assumptions (see Paper II), the 'BT' model can be obtained from the 'T2' model. Recently it has been shown (Kramer & Wex, private communication) that the 'DD' model provides poor uncertainties for measurements of the orbital Shapiro delay when the orbital inclination $i \sim 90°$. In the 'T2' model (and the 'DDS' model) a new parameter $x \equiv -\ln(1 - \sin i)$ can be used for such edge-on binary systems. As shown by Kramer (private communication) TEMPO2 provides more reliable estimates of the uncertainty on the new parameter x (known as SHAPMAX as it relates to the maximum Shapiro delay for a near-circular orbit) than on $\sin i$ for near edge-on binary systems. For instance, with our observations of PSR J1909−3744, the 'DD' model gives a companion mass of $m_{\rm c} = 0.2061(16)\,{\rm M}_\odot$ and $\sin i = 0.998\,20(8)$. The 'T2' model gives $m_{\rm c} = 0.2063(17)\,{\rm M}_\odot$ and $x = 6.28(6)$ implying that $\sin i = 0.998\,13(11)$. Fig. 14 gives a χ^2 plot indicating the fitted parameters obtained using the 'T2' and 'DD' models.

The 'T2' model, by default, returns theory-independent results. However, it is possible to assume that general relativity applies, emulating the 'DDGR' model developed by Taylor (1987) and Taylor & Weisberg (1989) for TEMPO1. This allows the determination of the mass of the pulsar and its companion.

For wide-orbit binary systems, Kopeikin (1995) showed that orbital timing parallaxes are measurable. Kopeikin (1996) also described secular variations of orbital parameters due to the system's proper motion. These terms are included as part of the 'T2' model, but require an estimate of the longitude of the ascending node of the binary's orbit, Ω.

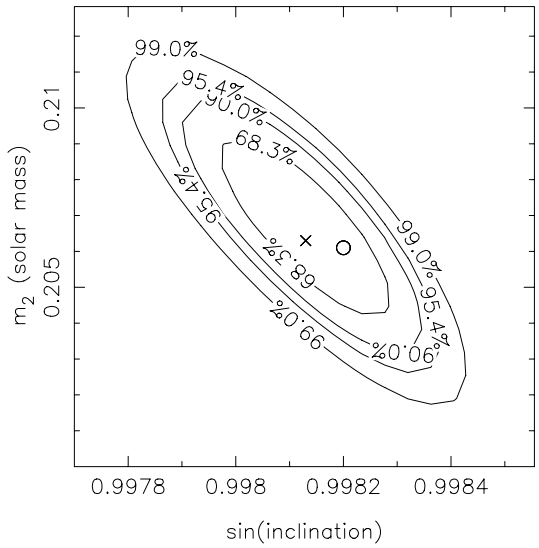

Figure 14. χ^2 contours in m_2 −sin i parameter space for PSR J1909−3744. The circle indicates the most-likely values obtained using the 'DD' model and the cross symbol for the 'T2' model. This plot was produced using the M2SINI plug-in.

Table 7. Binary orbital parameters included in TEMPO2.

Parameter	Description	Symbol
PB	Binary period of pulsars (d)	$P_{\rm b}$
ECC	Eccentricity of orbit	e
A1	Projected semimajor axis of orbit (lt-s)	x
T0	Epoch of periastron (MJD)	T_0
OM	Longitude of periastron ($^\circ$)	ω
TASC	Epoch of ascending node (MJD)	$T_{\rm asc}$
EPS1	$e \sin\omega$	η
EPS2	$e \cos\omega$	κ
KOM	longitude of the ascensing node	Ω
KIN	inclination angle	i
SHAPMAX	$-\ln(1-\sin i)$	s_x
OMDOT	Periastron advance (deg yr^{-1})	$\dot{\omega}$
PBDOT	The first time derivative of binary period	$\dot{P}_{\rm b}$
ECCDOT	Rate of change of eccentricity (s^{-1})	$\dot{e}$
A1DOT	Rate of change of semimajor axis (lt-s s^{-1})	$\dot{x}$
GAMMA	Post-Keplerian 'gamma' term (s)	γ
XPBDOT	Rate of change of orbital period minus GR prediction	
EPS1DOT	Rate of change of EPS1	$\dot{\eta}$
EPS2DOT	Rate of change of EPS2	$\dot{\kappa}$
MTOT	Total system mass ($M_\odot$)	M
M2	Companion mass ($M_\odot$)	m_2
DTHETA	Relativistic deformation of the orbit	d_θ
XOMDOT	Rate of periastron advance minus GR prediction (deg yr^{-1})	
SINI	Sine of inclination angle	s
DR	Relativistic deformation of the orbit	$d_{\rm r}$
A0	The first aberration parameter	A
B0	The second aberration parameter	B
BP	Tensor multiscalar parameter	β'
BPP	Tensor multiscalar parameter	β''
AFAC	Aberration geometric factor	
BPJEP_k	Epoch of a step-jump in the binary parameters	
BPJPH_k	Size of phase jump	
BTJPB_k	Size of jump in orbital period	
BTJA1_k	Size of jump in projected semimajor axis	
BTJECC_k	Size of jump in orbital eccentricity	
BTJOM_k	Size of jump in longitude of periastron	

The PSR B1259−63 system of a pulsar orbiting a Be star has proved difficult to model. Wang, Johnston & Manchester (2004) therefore developed the modified BT model that allowed for jumps in the Keplerian parameters at specified times (specifically, for this system, at periastron); such jumps are available in the 'T2' model. A more physical approach to the effect of non-point-mass companions was developed by Wex (1998) through alterations in the secular behaviour of the longitude of periastron and the projected semimajor axis. These changes are also available as part of the 'T2' binary model.

For orbits with small eccentricities, the 'T2' model, by default, produces highly covariant values for the epoch and the longitude of periastron. The 'ELL1' model of Wex (1998 unpublished work; see Lange et al. 2001) was developed for pulsars in such orbits. TEMPO2 provides a tool to convert between a timing model based on the BT model and one based on the ELL1 model which is defined by the parameters

$$\mathrm{EPS1} = e \sin\omega \tag{12}$$

$$\mathrm{EPS2} = e \cos\omega \tag{13}$$

$$\mathrm{TASC} = T_0 - \frac{\omega}{2\pi} P_{\rm b} \tag{14}$$

where e represents the orbital eccentricity, ω the longitude of periastron, T_0 the epoch of periastron and $P_{\rm b}$ the orbital period. If these parameters are included in a 'T2' parameter file, then the 'T2' model will emulate the 'ELL1' model.

These binary models provide the ability to determine the Keplerian parameters of the orbit and various post-Keplerian parameters (listed in Table 7). From the fitted values, TEMPO2 can provide various derived quantities including the mass function

$$f = \frac{(m_{\rm c} \sin i)^3}{(m_{\rm p} + m_{\rm c})^2} = \frac{4\pi^2}{G} \frac{(a_{\rm p} \sin i)^3}{P_{\rm b}^2}. \tag{15}$$

By assuming a typical pulsar mass of $m_{\rm p} = 1.35\,M_\odot$, a lower limit on the companion mass can be estimated by assuming that the orbit is viewed edge-on ($i = 90^\circ$), a median mass ($i = 60^\circ$) and an upper bound at the 90 per cent confidence level from $i = 26.^\circ0$ (see, e.g. Lorimer & Kramer 2005). These values are obtained by solving the mass function for the companion mass, $m_{\rm c}$, using a Newton–Raphson method. If $\sin i$ and $m_{\rm c}$ are known (e.g. from Shapiro delay measurements), then the mass function gives the pulsar mass.

5.4 Determining pulsar parameters

Timing models contain the pulsar's rotational, positional and binary parameters at a specific epoch. It is often useful to determine such parameters at a different epoch. TEMPO2 provides tools to calculate the parameters at any given epoch. The position (α, δ) in equatorial coordinates are updated from the position epoch using proper motion determinations $(\mu_\alpha \cos\delta, \mu_\delta)$

$$\alpha' = \alpha + \frac{\mu_\alpha \Delta t_A}{\cos\delta} \tag{16}$$

$$\delta' = \delta + \mu_\delta \Delta t_A \tag{17}$$

where Δt_A represents the difference between the requested epoch and the current model position epoch.

The pulsar's spin frequency and its first derivative are updated from the first and subsequent frequency derivatives

$$\nu' = \nu + \dot{\nu}\Delta t_{\rm P} + \frac{1}{2}\ddot{\nu}(\Delta t_{\rm P})^2 + \ldots \tag{18}$$

$$\dot{\nu}' = \dot{\nu} + \ddot{\nu}\Delta t_{\rm P} + \ldots \tag{19}$$

where $\Delta t_{\rm P}$ represents the change between the requested epoch and the current epoch for the given frequency determinations.

Binary parameters are more problematic. The epoch of periastron T_0 (or the epoch of the ascending node, $T_{\rm asc}$) is updated to the closest periastron to the requested epoch by calculating the nearest integer n to

$$a_n = \frac{\Delta t_{\rm b}}{P_{\rm b}} - \frac{1}{2}\dot{P}_{\rm b}\left(\frac{\Delta t_{\rm b}}{P_{\rm b}}\right)^2 \tag{20}$$

which represents the number of orbits since the timing model epoch of periastron T_0, that is, in interval $\Delta t_{\rm b}$. The epoch of periastron is subsequently updated

$$T_0' = T_0 + (\Delta t_{\rm b})' \tag{21}$$

where $(\Delta t_{\rm b})'$ is obtained by solving equation (20) with $a_n = n$. The orbital period $(P_{\rm b})$, longitude of periastron (ω), eccentricity (e) and projected semimajor axis (a_1) are updated as

$$P_{\rm b}' = P_{\rm b} + \dot{P}_{\rm b}(\Delta t_{\rm b})' \tag{22}$$

$$\omega' = \omega + \dot{\omega}(\Delta t_{\rm b})' \tag{23}$$

$$e' = e + \dot{e}(\Delta t_{\rm b})' \tag{24}$$

$$a_1' = a_1 + \dot{a}_1(\Delta t_{\rm b})' \tag{25}$$

5.5 Publishing timing ephemerides

TEMPO1 provided only limited output formats for the timing model parameters. The PUBLISH plug-in for TEMPO2 provides the user with the ability to produce output in a LaTeX table format (as in Table 8 where, in this case, the uncertainty on each parameter for PSR J0437−4715 has been multiplied by a factor of 2 and the error corresponds to the uncertainty on the last quoted digit).

If many parameters are included in the fit, then it is possible that the resulting uncertainties are covariant. This can be checked using the MATRIX plug-in that displays the correlation matrix for the fit (a typical output is shown in Table 9 for PSR J0437−4715). It is common for low-eccentricity binary pulsars that the epoch of periastron and the longitude of periastron are near-degenerate. It is common in publications to quote highly covariant parameters with more precision than suggested by the formal errors (see e.g. Ryba & Taylor 1991), however, the use of the ELL1 binary model is preferred.

Table 8. Example parameters in a LATEX table format for PSR J0437−4715 obtained using the PUBLISH plug-in.

Fit and data set	
Pulsar name	J0437−4715
MJD range	53041.3−53767.3
Number of TOAs	603
Rms timing residual (μs)	1.6
Weighted fit	*N*
Measured quantities	
Right ascension	04:37:15.78858(13)
Declination	−47:15:08.4685(15)
Pulse frequency (s^{-1})	173.687 946 306 02(7)
First derivative of pulse frequency (s^{-2})	$-1.7292(4)\times10^{-15}$
Dispersion measure ($cm^{-3}pc$)	2.641 23(17)
Proper motion in Right ascension (mas yr^{-1})	120.9(3)
Proper motion in Declination (mas yr^{-1})	−71.0(3)
Parallax (mas)	8(3)
Orbital period (d)	5.741 046 4584(16)
Epoch of periastron (MJD)	511 94.620(6)
Projected semi-major axis of orbit (lt-s)	3.36670624(19)
Longitude of periastron (°)	0.9(4)
Orbital eccentricity	0.000 018 99(11)
Set quantities	
Epoch of frequency determination (MJD)	511 94
Epoch of position determination (MJD)	511 94
Epoch of dispersion measure determination (MJD)	511 94
Sine of inclination angle	0.6788
First derivative of orbital period	3.64×10^{-12}
Periastron advance (deg yr^{-1})	0.016
Companion mass ($M_\odot$)	0.236
Derived quantities	
$\log_{10}$(Characteristic age, yr)	9.20
$\log_{10}$(Surface magnetic field strength, G)	8.76
Assumptions	
Clock-correction procedure	TT(TAI)
Solar system ephemeris model	DE405
Binary model	DD
Model version number	5.00

Note. Figures in parentheses are twice the nominal 1σ TEMPO2 uncertainties in the least-significant digits quoted.

Published timing parameters are used to make predictions for on-line observations of pulsars, for comparing results between different observing systems and for searching for variations in the parameters with time. It is therefore essential that full details of how the timing model was created are published alongside the parameters. For any published timing parameters it is necessary to (1) indicate whether the uncertainties represent 1 or 2σ formal errors on the fitted parameters and whether a weighted or non-weighted fitting procedure was used; (2) specify the Solar system ephemeris used; (3) indicate the TEMPO2 version number and describe which of the default TEMPO2 algorithms have not been used and which non-default algorithms included; (4) provide full information of any pre-whitening carried out on the data set; (5) define the coordinate system used; and (6) provide details of the clock correction process. The fitting process should be iterated until the pre- and post-fit values are identical indicating that the fit has converged. If a weighted fit is carried out, then it is necessary, in order to obtain accurate errors on the fitted

Table 9. The correlation matrix for the fitted parameters for PSR J0437−4715 data obtained using the MATRIX plug-in for TEMPO2. The global correlation (gcor) parameter is a measure for the strongest correlation between the fitted variable and a linear combination of all other variables. $\mathrm{dp} = -\log_{10}(1 - \mathrm{gcor}^2)^{1/2}$ provides an estimate of the number of 'insignificant' digits that should be quoted in a timing solution; see text.

	F0	T0	A1	OM	ECC
F0	+1.000 000 00				
T0	−0.134 746 57	+1.000 000 00			
A1	+0.113 938 21	+0.008 416 76	+1.000 000 00		
OM	−0.134 746 30	+0.999 999 98	+0.008 416 40	+1.000 000 00	
ECC	+0.007 090 55	+0.183 550 36	+0.106 756 29	+0.183 550 54	+1.000 000 00
gcor	+0.178 350 63	+0.999 999 98	+0.155 664 51	+0.999 999 98	+0.212 517 47
dp	0.1	7.8	0.1	7.8	0.1

parameters, to ensure that the reduced χ^2-value of the fit is close to unity. It is also a common practice and desirable to convert the measured parameters so that the period, position and binary epochs refer to the centre of the data span.

6 ANALYSING THE TIMING RESIDUALS

Any systematic feature in the post-fit timing residuals indicates that some effect is not being described by the timing model. Analysing such features potentially provides important information about various perturbations, including the presence of planetary companions, variations in the ISM, precession of the neutron star or irregularities in the pulsar's rotation and spin-down. The timing residuals can also provide an indication that the TOAs are affected by calibration problems or other instrumental effects.

The pre- and post-fit timing residuals can be plotted in numerous ways. For instance, the PLK plug-in allows the user to plot the residuals versus parameters such as day, observing frequency, binary phase, observation length or the parallactic angle. Other plug-ins allow the user to obtain a list of the timing residuals, barycentric arrival times, clock corrections etc. in a specified tabular format.

As the true uncertainty on any fitted parameter is the combination of the random and systematic errors, it is necessary to attempt to quantify the effects of the systematic errors present in the data. Ryba & Taylor (1991) discussed two methods to do this which are implemented in the ERRORS plug-in.

(i) It is possible to plot a histogram of the normalized post-fit residuals (the value of the residual divided by its estimated uncertainty). If this histogram follows a Gaussian distribution, then it is likely that the data are not significantly affected by systematic effects (Fig. 15a).

(ii) Compute averages of consecutive sets 1, 2, 4, 8 and 16 normalized residuals and plot the standard deviations within each group. Random Gaussian measurement errors produce deviations $\propto 1/\sqrt{N}$ where N is the number of residuals averaged (Fig. 15b).

TEMPO2 plug-ins provide numerous tools for analysing the post-fit timing residuals or for outputting the residuals in formats that are suitable for other data-analysis packages. We have noted that large numbers of packages have been created to analyse timing residuals from the output files of the TEMPO1 software and therefore provide facilities within TEMPO2 to produce output files with the same format as TEMPO1. However, it is relatively straightforward to develop new plug-ins or to convert old software for use by TEMPO2. For instance, a template plug-in is available which users can modify for their own specific uses. Many such plug-ins to analyse the post-fit timing residuals are currently being designed or tested. Examples include the implementation of a multiresolution CLEAN deconvolution algorithm and periodicity searches (M. Rissi, private communication).

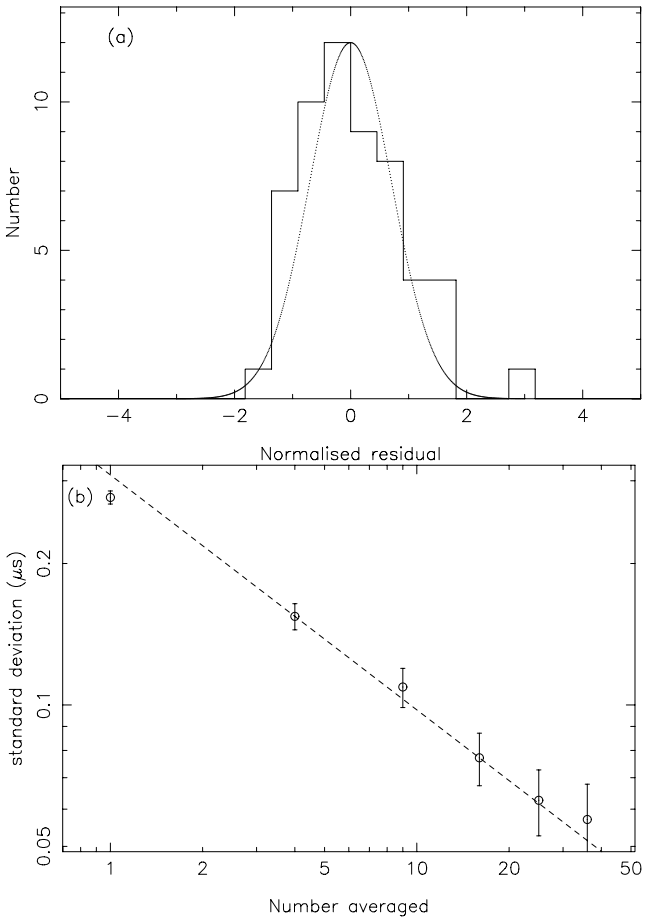

Figure 15. (a) Normalized residuals for PSR J1909−3714 plotted as a histogram with a Gaussian curve overlaid. (b) rms timing residuals after averaging different numbers of residuals together with a line indicating the expected $\sqrt{N}$ dependence. These plots were created using the ERRORS plug-in.

7 PREDICTIVE MODE

The folding of pulsar signals proceeds on the basis of the predicted time-evolution of the phase of the pulse train incident upon the

observatory. The timing model specifies this evolution, but is too computationally intensive for real-time applications. Like TEMPO1, TEMPO2 is able to produce a polynomial approximation of the phase, $\phi(t)$, and pulse frequency, ν, over specified time intervals. The number of coefficients and the time-span fitted can be set by the user; TEMPO2 provides a warning message if the rms deviation between the model and the data is large and more coefficients or a shorter span is necessary.

7.1 TEMPO1-compatible polynomials

To ease the transition from TEMPO1 to TEMPO2, a facility is provided to produce predictive polynomials in the same format as those made by TEMPO1. These consist of a series of sets of coefficients of polynomials that approximate the evolution of pulse phase incident upon the specified observatory. Owing to interplanetary and interstellar dispersion, the polynomial is specific to a given observing frequency. For observations at radio wavelengths, there is usually a significant variation of instantaneous pulse phase across the observing band. If high precision is required, the form of this variation is dependent on many parts of the full timing model, thereby defeating any gains in simplicity offered by substituting a polynomial form for the time-evolution. For this reason, TEMPO2 can produce new time- and frequency-dependent predictive polynomials (Section 7.2) which are recommended for precision applications.

A simplified approximation to the frequency dependence may be used in less-critical applications. For isolated pulsars, the difference in time of emission between radiation received simultaneously at an observing frequency, f, and the frequency for which the polynomial applies, f_0, is

$$\Delta_D = D\left(f^{-2} - f_0^{-2}\right), \tag{26}$$

where D is the dispersion constant (Section 3.5). Neglecting any variation in pulse frequency over the interval Δ_D (safe for isolated pulsars), the resultant phase difference is simply $\nu\Delta_D$, where ν is the pulse frequency at the epoch of consideration. The pulse frequency in the reference frame of the observatory is simply obtained from the polynomial, and the observing frequency is also generally known by its value in the observatory frame. It is therefore convenient to perform the calculation in this frame, after transforming the dispersion constant (D, with dimensions of time^{-1}) using the 'Doppler shift'[9] value (β) specified in the polynomial data file:

$$\phi(t, f) \simeq \phi(t, f_0) - \nu(t, f_0)\left(f^{-2} - f_0^{-2}\right)\frac{D}{1+\beta}. \tag{27}$$

To the best of our knowledge, the application of β to the dispersion constant is often neglected in existing de-dispersion software, incurring an error of up to $\sim\Delta_D \times 10^{-4}$, typically of the order of several microseconds. It should also be noted that unlike TEMPO2, the value of the DM provided in TEMPO1 polynomial files does not include the interplanetary contribution, typically in the range 100 ns to 100 μs.

For isolated pulsars, the limiting factor in the accuracy of this approach is the time-evolution of the transformation between the observatory and barycentric frames ($1 + \beta$). Only a single value is provided for each polynomial, which typically spans several hours. The rotation of the Earth accelerates the observatory sufficiently to change β at rates of up to $\sim 10^{-10}$ s^{-1}, resulting in errors of the order of tens of nanoseconds. Fig. 16 illustrates the effect.

[9] In TEMPO2 the rate correction also includes gravitational redshift and time-dilation.

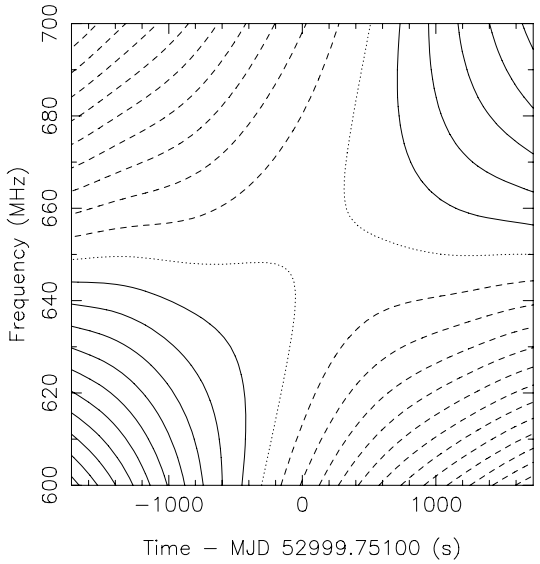

Figure 16. Contour map of the difference between the pulse phase as predicted by the full TEMPO2 timing model, versus a single-frequency polynomial approximation in conjunction with equation (27), for an hour-long observation of the binary pulsar PSR J1906+0746 with $f_0 = 650$ MHz. Contours are spaced by 5 ns; dashed contours are negative, positive contours are solid and the zero contour is dotted. Two main effects are noticeable. The largest effect is due to the evolution in the observatory Doppler shift, manifested as a monotonic function of time and frequency [delay $\propto t(f^{-2} - f_0^{-2})$, where t is the time relative to the observation midpoint]. The second, smaller effect is due to second- and higher-order terms in the orbital motion of the pulsar [delay approximately $\propto (f^{-2} - f_0^{-2})^2$]. At the midpoint in time where the first effect vanishes, the second effect appears as a form roughly quadratic in frequency offset. Elsewhere it contributes to the overall asymmetry of the difference function.

For binary pulsars, more severe effects are encountered, owing to the different orbital phases of emission of radiation received simultaneously at different frequencies. The most striking result of this is that, for observing frequencies well away from the frequency assumed in the construction of the polynomial, pulse profile peaks lead or lag the prediction as a function of orbital phase. While eye-catching, to the extent that the error in the predicted pulse phase is constant over the course of a given integration, this effect should not manifest directly in the measured pulse-arrival times. Likewise, if pulse profile data are combined from several frequencies (or an observing band is coherently dedispersed), as long as 'de-dispersion' proceeds as prescribed in equation (27), the apparent orbital-phase-dependent effect is compensated to first order by the variation in the topocentric pulse frequency used to convert a dispersion time-delay to a phase delay. However, in addition to the secular drift of β, two remaining effects dictate the use of time- and frequency-dependent two-dimensional polynomials for precision timing of binary pulsars.

First, unless taken into account, the variation in apparent pulse frequency as a function of observing frequency can be large enough to cause appreciable smearing of the pulse profile if not taken into account. With scintillation, the smearing may be significantly asymmetric, resulting in errors in measured pulse times of arrival. The fractional change in pulse frequency is given to first order by $\Delta_D\, a/c$ where a is the line-of-sight orbital acceleration. See Fig. 17 for an example. Smearing widths for sample pulsars and observing configurations are listed in Table 10.

Secondly, if profiles from several frequencies are to be combined (or an observing band is to be coherently dedispersed), equation (27)

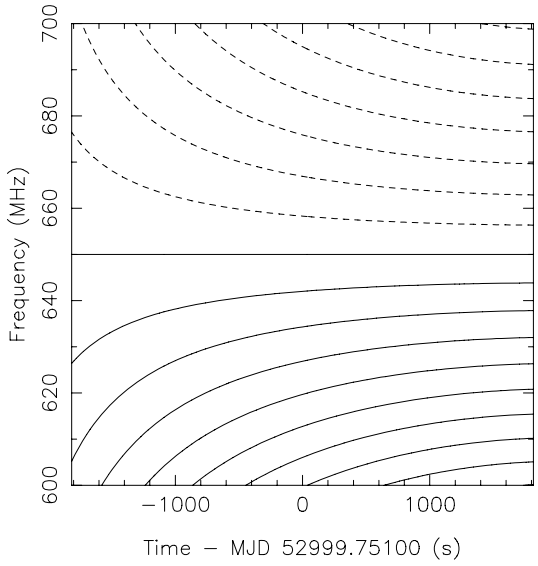

Figure 17. Contour map of the fractional difference in apparent pulse frequency at a given observing frequency, versus the central frequency (650 MHz), for an hour-long observation of the binary pulsar PSR J1906+0746. Contours are spaced at 10^{-8}, corresponding to 10 ns of smearing per second of integration. Dashed contours are negative.

corrects only to first order in Δ_D. Since the topocentric frequency, $\nu(t, f)$ itself varies with dispersion delay, the second-order term (expressed as a time-delay) is given by $\Delta_D^2\ a/2c$. This effect is apparent in Fig. 16, especially around $t = 0$ where the differential Doppler effect vanishes. The magnitudes of the effect for sample pulsars and observing configurations are provided in Table 10.

7.2 Time- and frequency-dependent predictions

To overcome the limitations of the TEMPO1-type predictive polynomial described in the previous section, TEMPO2 is able to compute a two-dimensional polynomial approximation to the timing model, with time and observing frequency as its arguments. This mode is recommended for precision applications in future processing systems.

The polynomial is expressed in terms of a two-dimensional adaptation of the conventional Chebyshev basis functions:

$$p_{ij}(x, y) = \cos(i \cos^{-1} x) \cos(j \cos^{-1} y). \quad (28)$$

Analogous to the one-dimensional case, a discrete form of a set of such basis functions is orthogonal if computed on a grid of $M \times N$ coordinates (x_i, y_j) satisfying

$$\cos(M \cos^{-1} x_i) \cos(N \cos^{-1} y_j) = 0. \quad (29)$$

The coefficients of the polynomial approximation to a function $g(x, y)$ are therefore easily computed via the inner product:

$$c_{kl} = \frac{4}{MN} \sum_{i=1}^{M} \sum_{j=1}^{N} p_{kl}(x_i, y_j) g(x_i, y_j). \quad (30)$$

This yields an approximation function

$$g(x, y) \simeq \sum_{k=1}^{M} \sum_{l=1}^{N} c_{kl}\, p_{kl}(x, y), \quad (31)$$

which is exact for x, y coordinates satisfying equation (29). For computation, this can be rewritten as a one-dimensional Chebyshev polynomial with another Chebyshev polynomial defining its coefficients:

$$g(x, y) \simeq \sum_{l=1}^{N} T_l(y) \sum_{l=1}^{N} T_k(x) c_{kl}, \quad (32)$$

where the one-dimensional basis functions, $T_k(x) = \cos(k \cos^{-1} x)$, can be computed efficiently using Clenshaw's recurrence relation (Press et al. 1992).

After mapping the requested intervals in time and observing frequency to x and y in the interval $[-1, 1]$, TEMPO2 computes the coefficients c_{kl} approximating the function $\phi(t,\ f)\ -k f^{-2}$, where k is a constant computed to remove the bulk of the frequency dependence due to interstellar dispersion. Subtraction of this term significantly reduces the number of coefficients needed for an accurate approximation. The $M \times N$ coefficients and the constant k are written to file to allow the later construction of the approximation of $\phi(t, f)$ without reference to the full timing model.

Table 10. Smearing and phase errors with TEMPO1-style predictive polynomials for sample pulsars.

Name	P (ms)	DM (cm pc^{-3})	$a \sin i$ (lt-s)	$P_{\rm orb}$ (d)	$\Delta_1{}^b$ (ns)	Δ_1/P (10^{-6})	$\Delta_2{}^b$ (ns)	Δ_2/P (10^{-6})
J1906+0746	144.1	217.8	1.42	0.17	10 100	70	18.8	0.13
J0737−3039A	22.7	48.9	1.42	0.10	6000	260	2.5	0.11
B1744−24A	11.6	242.2	0.12	0.08	4600	400	9.4	0.8
B1913+16	59.0	168.8	2.34	0.32	3400	58	4.9	0.08
J1756−2251	28.5	121.2	2.76	0.32	2900	100	3.0	0.11
J1802−2124	12.6	149.6	3.72	0.70	1000	81	1.3	0.10
J1435−6100	9.3	113.7	6.18	1.35	345	37	0.3	0.04
J0218+4232	2.3	61.3	1.98	2.03	26	11	14×10^{-3}	6×10^{-3}
B1957+20	1.6	29.1	0.09	0.38	16	10	4×10^{-3}	2×10^{-3}
J1909−3744	2.9	10.4	1.90	1.53	7.6	2.6	6×10^{-4}	2×10^{-4}
J2145−0750	16.1	9.0	10.16	6.84	1.8	0.11	14×10^{-5}	8×10^{-6}
B1855+09	5.4	13.3	9.23	12.33	0.7	0.14	8×10^{-5}	15×10^{-6}
J0437−4715	5.8	2.6	3.37	5.74	0.2	0.04	1×10^{-5}	10^{-6}

[a]Maximum smearing due to pulse frequency offset at $f = 600$ MHz versus $f_0 = 650$ MHz, over 100-s integration (see text). Note, values are approximate only: orbital eccentricity neglected.
[b]Maximum timing error due to neglected order-Δ_D^2 term, for $f = 600$ MHz, $f_0 = 650$ MHz (see text).

Using this approach, the timing model, including its frequency dependence, can be approximated to subnanosecond accuracy using a modest number of coefficients. As an example, the phase evolution of PSR J1906+0746 over the time and frequency interval depicted in Fig. 16 requires nine coefficients in the time-axis and six in frequency, yielding a difference function with an rms variation of 450 ps. For an observation of an isolated pulsar, over the same time interval and frequency band, only 5×3 coefficients are needed to model the time- and frequency-dependent variations in phase, which apart from the basic pulsar frequency, are dominated by the acceleration of the observatory due to the rotation of the earth.

The software library packaged with TEMPO2 provides routines for evaluating the predicted pulse phase and pulse frequency as a function of time and observing frequency. For convenience in applications involving folding of pulsar time-series data, the software can also produce a piecewise linear approximation which minimizes the mean error and keeps the rms within specified bounds. A plug-in called POLYTEST is also provided to assess the accuracy of a computed polynomial (either one- or two-dimensional), reporting on the rms and extrema of the residuals and producing plots such as those in Figs 16 and 17.

8 SUMMARY AND CONCLUSION

In summary, we list below the improved features of TEMPO2 compared to TEMPO1. For coordinate systems, propagation delays and ephemerides, TEMPO2

(i) is compliant with IAU 2000 resolutions and implements updated precession and nutation models, polar motion, the ICRS coordinate system and BCT (SI units) instead of BDT;
(ii) corrects the observing frequency for relativistic time-dilation;
(iii) uses an improved tabulation of the Solar system Einstein delay;
(iv) includes atmospheric propagation delays;
(v) includes the Shapiro delay due to the planets; and
(vi) includes the second-order Shapiro delay due to the Sun.

For the fitting routines, TEMPO2

(i) has the ability to simultaneously fit to the timing residuals of multiple pulsars;
(ii) implements frequency-dependent fitting (not only DM delays);
(iii) has the ability to fit for DM at each epoch using simultaneous observations;
(iv) allows fits for an arbitrary number of pulse frequency derivatives, DM derivatives and glitches;
(v) simplifies and provides flexible methods for placing arbitrary offsets between TOAs obtained at different frequencies or observatories;
(vi) can whiten data using harmonically related sinusoids;
(vii) provides a brute-force method for obtaining timing solutions;
(viii) fully includes the effects of secular motion of the pulsar; and
(ix) includes the orbital parallax terms in binary models.

The predictive mode in TEMPO2 provides both time- and frequency-dependent predictions and therefore deals correctly with

(i) the Earth rotation; and
(ii) binary motion.

Other miscellaneous improvements include

(i) generalized input formats;
(ii) generalized output formats;
(iii) the ability to simulate pulse-arrival times;
(iv) the implementation of numerous graphical interfaces;
(v) calculating the post-fit residuals (instead of predicting them);
(vi) the ability to update binary parameters to a given epoch; and
(vii) generalized clock-correction routines.

We have presented a new software package, TEMPO2, that supersedes the existing TEMPO package. TEMPO2 has been analysed in detail and we believe that all the corrections to the measured TOAs that have been implemented are accurate to better than 1 ns. The software has been designed so that it is easy to modify current routines and to add new functions to describe phenomena which affect pulsar-timing residuals. For instance, a user can easily implement a new binary model or create a personal graphical interface.

The TEMPO2 framework is such that it is relatively easy to fit global parameters across multiple data sets. This will be the topic of a forthcoming paper and will be used in the hunt for gravitational waves, refining the Solar system ephemeris and establishing a pulsar-based time-scale.

ACKNOWLEDGMENTS

The TEMPO2 package is based on the original TEMPO FORTRAN code. This software was developed over many years by multiple authors including J. Taylor, R. Manchester, D. Nice, W. Peters, J. Weisberg, A. Irwin and N. Wex. We thank the Australian pulsar community, J. Weisberg, D. Lorimer and M. Kramer for suggestions and comments on TEMPO2. The data presented in this paper were obtained as part of the PPTA project that is a collaboration between the ATNF, Swinburne University and The University of Texas, Brownsville, and we thank our collaborators on this project. The Parkes radio telescope is part of the Australia Telescope which is funded by the Commonwealth of Australia for operation as a National Facility managed by CSIRO.

REFERENCES

Backer D. C., Hellings R. W., 1986, ARA&A, 24, 537
Backer D. C., Hama S., Hook S. V., Foster R. S., 1993, ApJ, 404, 636
Bell J. F., Bailes M., 1996, ApJ, 456, L33
Blandford R., Teukolsky S. A., 1976, ApJ, 205, 580
Damour T., Deruelle N., 1986, Ann. Inst. H. Poincaré (Physique Théorique), 44, 263
Damour T., Taylor J. H., 1991, ApJ, 366, 501
Feissel M., Mignard F., 1998, A&A, 331, L33
Folkner W. M., Charlot P., Finger M. H., Williams J. G., Sovers O. J., Newhall X. X., Standish E. M., 1994, A&A, 287, 279
Foster R. S., Backer D. C., 1990, ApJ, 361, 300
Foster R. S., Cordes J. M., 1990, ApJ, 364, 123
Guinot B., 1988, A&A, 192, 370
Harada W., Fukushima T., 2004, AJ, 127, 531
Hilton J. L., Hohenkerk C. Y., 2004, A&A, 413, 765
Hobbs G., Lyne A. G., Kramer M., Martin C. E., Jordan C., 2004, MNRAS, 353, 1311
Hobbs G., Lorimer D. R., Lyne A. G., Kramer M., 2005, MNRAS, 360, 974
Irwin A. W., Fukushima T., 1999, A&A, 348, 642
Issautier K., Meyer-Vernet N., Moncuquet M., Hoang S., 1998, J. Geophys. Res., 103, 1969
Jenet F. A., Hobbs G. B., Lee K. J., Manchester R. N., 2005, ApJ, 625, L123
Klioner S. A., 2005, preprint (astro-ph/0508292)

Kopeikin S. M., 1995, ApJ, 439, L5
Kopeikin S. M., 1996, ApJ, 467, L93
Lange C., Camilo F., Wex N., Kramer M., Backer D., Lyne A., Doroshenko O., 2001, MNRAS, 326, 274
Lieske J. H., Lederle T., Fricke W., Morando B., 1977, A&A, 58, 1
Lorimer D., Kramer M., 2005, Handbook of Pulsar Astronomy. Cambridge Univ. Press, Cambridge
Lyne A. G., 1999, in Arzoumanian Z., van der Hooft F., van den Heuvel E. P. J., eds, Pulsar Timing, General Relativity, and the Internal Structure of Neutron Stars. Koninklijke Nederlandse Akademie van Wetenschappen, Amsterdam, p. 141
Lyne A. G., Smith F. G., 1998, Pulsar Astronomy, 2nd edn. Cambridge Univ. Press, Cambridge
Lyne A. G. et al., 2004, Sci, 303, 1153
Manchester R. N., Taylor J. H., 1977, Pulsars. Freeman, San Francisco
McCarthy D. D., Luzum B. J., 2003, Celest. Mech. and Dynamical Astron., 85, 37
Petit G., 2003, in Capitaine N., ed., Journées 2001 - Systèmes de Référence Spatio-Temporels. Influence of Geophysics, Time and Space Reference Frames on Earth Rotation Studies. ESA Publications Division, Noordwijk, 163
Phillips J. A., Wolszczan A., 1992, ApJ, 385, 273
Press W. H., Teukolsky S. A., Vetterling W. T., Flannery B. P., 1992, Numerical Recipes: The Art of Scientific Computing, 2nd edn. Cambridge Univ. Press, Cambridge
Ryba M. F., Taylor J. H., 1991, ApJ, 380, 557
Seiber W., 1982, A&A, 113, 311
Seidelmann P. K., Kovalevsky J., 2002, A&A, 392, 341
Shapiro I. I., 1964, Phys. Rev. Lett., 13, 789
Shklovskii I. S., 1970, SvA, 13, 562
Spitzer L., 1962, Physics of Fully Ionized Gases. Interscience, New York
Splaver E. M., Nice D. J., Stairs I. H., Lommen A. N., Backer D. C., 2005, ApJ, 620, 405
Stairs I. H., 2003, Living Reviews in Relativity, 6, 5
Standish E. M., 1990, A&A, 233, 252
Standish E. M., 1998, A&A, 336, 381
Taylor J. H., 1987, in Helfand D. J., Huang J.-H., eds, IAU Symp., 125, The Origin and Evolution of Neutron Stars. Reidel, Dordrecht, p. 383
Taylor J. H., Weisberg J. M., 1989, ApJ, 345, 434
van der Swaluw E., 2003, A&A, 404, 939
van Straten W., 2003, PhD thesis, Swinburne University of Technology
Wall J. V., Jenkins C. R., 2003, Practical Statistics for Astronomers. Cambridge Univ. Press, Cambridge
Wang N., Johnston S., Manchester R. N., 2004, MNRAS, 351, 599
Wex N., 1998, MNRAS, 298, 67
Wolszczan A., Frail D. A., 1992, Nat, 355, 145

APPENDIX A: LIST OF PLUG-IN PACKAGES AVAILABLE FOR TEMPO2

(i) BASIC, plots a P–$\dot{P}$ diagram and indicates the position of the pulsar being analysed. Options are available to also display a sky-projection that indicates the pulsar's position and derived parameters such as the pulsar's characteristic age and surface dipole magnetic field strength are determined.

(ii) COMPARE, accepts two input parameter files and provides routines to compare differences between the residuals obtained using the two models. For instance, this interface can be used to compare the effects of different clock or ephemeris files or different binary models.

(iii) COMPARERES, accepts two input arrival-time files and provides routines to compare differences between the residuals.

(iv) DELAYS, shows the TEMPO2 calculated delays being added to the measured arrival times. For instance, clock corrections, ephemeris delays and dispersion delays are included.

(v) ERRORS, used to study systematic and random errors in the timing residuals.

(vi) FAKE, allows the user to create simulated arrival times that fit a given timing model. The addition of red and white-noise is possible.

(vii) GENERAL, a user-specified output format for the pre- and post-fit parameters.

(viii) GENERAL2, a user-specified output format for displaying the site and barycentric arrival times, the timing residuals and various clock and propagation corrections.

(ix) GORILLA, finds timing solutions using a brute-force method.

(x) LIST, provides a listing of the arrival times, residuals, clock corrections and propagation delays.

(xi) MATRIX, displays the correlation matrix of the fitted parameters.

(xii) PLK, an interface that plots the timing residuals versus parameters such as day, binary phase, length of observation etc. Various functions are available including the ability to highlight selected points, view pulse profiles and to delete observations and refit the data.

(xiii) POLYTEST, provides diagnostics of the approximation error of a predictive polynomial, including minimum, maximum and rms and frequency- and time-dependent contour maps.

(xiv) PUBLISH, produces publication-quality LATEX tables of the parameters.

(xv) SPECTRAL, provides basic spectral analysis tools for the timing residuals – including periodograms, auto-correlation functions and CLEAN deconvolution.

(xvi) SPLK, allows the plotting of multiple pulsar-timing residuals simultaneously.

(xvii) STATS, output mode that provides basic information about the pulsar and its fit. This plug-in gives the rms residuals for each observing frequency available.

(xviii) STRIDEFIT, allows fitting of subsets of adjacent observations. The resulting fit parameters can be stored and subsequently plotted versus time.

(xix) TRANSFORM, transforms a timing model created using TEMPO1 to one using the BCT time-scale and hence suitable for use with TEMPO2.

This paper has been typeset from a TEX/LATEX file prepared by the author.